Exploiting effector - host interactions using TurboID-based proximity labeling

Wei Shi [1,4], Sara C Stolze [2], Hirofumi Nakagami [2,3], Johana C. Misas Villamil [1,4], Isabel ML Saur [1,4], and Gunther Doehlemann [1,4]

1. Institute for Plant Sciences University of Cologne, Cologne, D-50674, Germany
2. Protein Mass Spectrometry, Max-Planck Institute for Plant Breeding Research, Carl-von-Linné-Weg 10, 50829 Cologne, Germany
3. Basic Immune System of Plants, Max-Planck Institute for Plant Breeding Research, Carl-von-Linné-Weg 10, 50829 Cologne, Germany
4. Cluster of Excellence on Plant Sciences (CEPLAS)

Author for correspondence: g.doehlemann@uni-koeln.de

Keywords: TurboID, fungal effectors, *Ustilago maydis*, maize, ubiquitin-proteasome.

Abstract

Plant pathogens secrete effectors, which target host proteins to facilitate infection. The *Ustilago maydis* effector UmSee1 is required for tumor formation in the leaf during infection of maize. UmSee1 interacts with maize SGT1 and blocks its phosphorylation *in-vivo*. In the absence of UmSee1, *U. maydis* cannot trigger tumor formation in the bundle sheath. However, it remains unclear which host processes are manipulated by UmSee1 and the UmSee1-SGT1 interaction to cause the observed phenotype. Proximity-dependent protein labeling involving the turbo biotin ligase tag (TurboID) for proximal labeling of proteins is a powerful tool for identifying the protein interactome. We have generated transgenic *U. maydis* that secretes biotin ligase-fused See1 effector (UmSee1-TurboID-3HA) directly into maize cells. This approach, in combination with conventional co-immunoprecipitation allowed to identify additional UmSee1 interactors in maize cells. Collectively, our data identified three ubiquitin-proteasome pathway-related proteins (ZmSIP1, ZmSIP2, ZmSIP3) that either interact with or are close to UmSee1 during host infection of maize with *U. maydis*. ZmSIP3 represents a cell cycle regulator which degradation appears to be promoted in the presence of UmSee1. Our data provide a possible explanation for the requirement of UmSee1 in tumor formation during *U. maydis* - *Zea mays* interaction.

Introduction

Most staple crops are essential for food security. Plant diseases greatly threaten food security by limiting the yield and quality of crops (Fisher *et al.*, 2016). Pathogens secrete effectors to target host structures for spreading infection (Dodds and Rathjen, 2010). Effectors usually modulate the biological activity of host proteins to suppress plant immunity (Hogenhout *et al.*, 2009). Identifying effector targets in the plant aids to the understanding of pathogenic mechanisms and thereby improves resistance to crop pathogens. The location, specificity, and low effector protein levels *in planta* are major obstacles for the identification of host target proteins.

Ustilago maydis is a plant fungal pathogen causing corn smut of many important crops and grasses, including the widely grown food and energy crop maize (*Zea mays*) (Kahmann and Kamper, 2004, Doehlemann *et al.*, 2008). *U. maydis* induces tumors on all aerial parts of maize and suppresses plant immunity by secreting effectors to the plant tissue (Skibbe *et al.*, 2010). Plant tumors produced upon *U. maydis* infection have been defined as clusters of cells that present abnormal cell division and reduced cell differentiation. The cell cycle is responsible for DNA replication and cell division and it is well-known that an abnormal cell cycle causes tumors in animals and plants (Jacobs *et al.*, 1999). *U. maydis* induces such tumors on all aerial parts of maize, which is a complex and dynamic process. The *U. maydis*-induced leaf tumor formation at the cellular level is composed of hypertrophic and hyperplasic tumor cells resulting from transformed mesophyll cells and bundle sheath cells, respectively (Matei *et al.*, 2018). About 460 effectors encoded by *U. maydis* target different host compartments (Lanver *et al.*, 2017). Only a few have been functionally characterized, including Pep1, Pit2, Cmu1, Tin2, See1, Mer1, Rip1 and Tips (Doehlemann *et al.*, 2009, Djamei *et al.*, 2011, Mueller *et al.*, 2013, Tanaka *et al.*, 2014, Redkar *et al.*, 2015a, Misas Villamil *et al.*, 2019, Darino *et al.*, 2021, Navarrete *et al.*, 2021, Bindics *et al.*, 2022, Saado *et al.*, 2022).

Interestingly, the organ-specific UmSee1 effector is required for the trans-differentiation of bundle sheath cells into hypertrophic tumor cells but not for the hypertrophic cells' enlargement in the mesophyll cells, and the UmSee1-induced tumor

63 formation and expansion only occur in vegetative tissues but not in floral tissues
64 (Redkar *et al.*, 2015a). The UmSee1 effector is translocated from biotrophic hyphae to
65 the plant cytoplasm and nucleus and a Yeast-two-Screen (Y2H) demonstrated the
66 interaction of UmSee1 with maize SGT1 (suppressor of G2 allele of skp1) (Redkar *et*
67 *al.*, 2015a). Several regulators control cell cycle progression, including cyclin-
68 dependent kinases (CDKs), cell division control proteins (CDCs), cyclin proteins
69 (CYCs), anaphase-promoting complex (APCs) and other activators or suppressors
70 (Dang *et al.*, 2021). The previously identified UmSee1-interactor SGT1 is required for
71 both the G1/S and G2/M cell cycle transitions in yeast and it is highly conserved in
72 eukaryotic cells (Kitagawa *et al.*, 1999). Although, UmSee1-mediated inhibition of
73 MAPK-triggered SGT1 phosphorylation could be detected (Redkar *et al.*, 2015a), it
74 remains elusive, how SGT1 affects the plant cell cycle and how the cell cycle is
75 influenced by UmSee1.
76 To give further insight into this key question and to minimize the individual limitations
77 of each protein-protein interaction assay, we complement the previously performed
78 Y2H screen (Redkar *et al.*, 2015a) with state-of-the-art *de novo* identification of
79 UmSee1 interactors *in planta*. We apply standard co-immunoprecipitation (Co-IP) and
80 establish proximity labeling (PL) for TurboID-catalyzed biotinylation of intracellular
81 maize proteins upon *U. maydis*-mediated delivery of TurboID-fused UmSee1. Co-IP is
82 very effective in obtaining stable complexes, but weak or transient interactors are not
83 detected (Ngounou Wetie *et al.*, 2014, Sciuto *et al.*, 2019). PL captures weak or transient
84 protein interactions and also proteins that locate consistently in close proximity of the
85 protein of interest (Gingras *et al.*, 2019). Biotin-based PL approaches have been applied
86 in yeast, plants and animals, including *Schizosaccharomyces pombe*, *Caenorhabditis*
87 *elegans*, *Arabidopsis thaliana* and *Nicotiana benthamiana*, using transient expression
88 or transgenic lines for specific cellular proteomes as well as interaction networks of
89 nuclear, cytosolic and membrane baits (Branon *et al.*, 2018, Conlan *et al.*, 2018,
90 Larochelle *et al.*, 2019, Mair *et al.*, 2019, Zhang *et al.*, 2019, Holzer *et al.*, 2022,
91 Melkonian *et al.*, 2022). In the present study, we used a transgenic *U. maydis* strain to
92 directly deliver UmSee1-TurboID-3HA fusion protein into maize cells during the

93 infection process. This approach obtained distinct datasets of putative UmSee1-
94 interacting candidates collectively suggesting a function of UmSee1 within the
95 ubiquitin-proteasome network, a pathway also involving SGT1 (Dielen *et al.*, 2010).
96 We selected three *Zea mays* UmSee1 interacting proteins (ZmSIPs) for further analysis
97 and found them to also associate with SGT1. All three ZmSIPs have been previously
98 implicated in the ubiquitin-proteasome pathway. Moreover, presence of UmSee1 is
99 linked to a more rapid degradation of ZmSIP3, a cell cycle regulator 48 (CDC48), by
100 the maize proteasome.
101

102 **Results**

103 **Establishment of TurboID-based proximity labeling in the *U. maydis*-maize**
104 **pathosystem**

105 A previous study demonstrated that UmSee1 is secreted into host cells during *U. maydis*
106 infection of maize leaves and that it can interact with the *Zea mays* SGT1 homolog
107 (Redkar *et al.*, 2015a). To explore the potential for identifying further UmSee1-
108 interacting proteins and proteins in close proximity to UmSee1 in maize leaves, we
109 aimed to directly transfer UmSee-TurboID-3HA fusion proteins from biotrophic fungal
110 hyphae into host cells (**Fig 1A**). We generated UmSee1 fused C-terminally to a
111 TurboID-3HA tag and expressed it under control of the *pit2* promoter, which confers a
112 high expression level in-planta (Doehlemann *et al.*, 2011). The construct
113 (*pPit2:UmSee1- TurboID -3HA,* **Fig 1B**) was expressed in the *see1* knock out strain
114 SG200Δsee1 strain which allowed to confirm that the recombinant effector protein fully
115 complemented the virulence defect of the SG200Δsee1 strain (**Fig 1C, Table S3**). Anti-
116 HA western blot analysis confirmed the successful enrichment of the fusion proteins
117 (**Fig 1D**). To select specificity in the following experiments, the mCherry protein was
118 fused to the signal peptide (SP) of UmSee1 (*pPit2:*SP_{UmSee1}*- mCherry-TurboID -3HA,*
119 **Fig 1B**) and expressed in *U. maydis* SG200, also under the *pit2* promoter. Maize leaves
120 infected with the two *U. maydis* strains and treated with free biotin were subjected to
121 protein extraction at three days post infection (dpi) under native (anti-HA) and
122 denaturing (TurboID) conditions. Plant protein extracts were subjected to anti-HA

immunoprecipitation and streptavidin-mediated isolation of biotinylated proteins, followed by liquid-chromatography mass spectrometry (LC-MS/MS) for the identification of isolated proteins (**Fig 1E**). Biotinylation of maize proteins by secreted UmSee1-TurboID-3HA was confirmed by strep-HRP western blot of raw protein extracts and streptavidin-enriched samples after treatment of the samples with 100 μM biotin (**Fig S1A**). Three biological replicates of Co-IP and TurboID were sampled from the identical plant for subsequent LC-MS/MS analysis. We detected enhanced biotinylation of maize proteins in all three replicates of samples carrying UmSee1 compared to the mCherry control samples (**Fig S1B**).

The relative amount of each identified protein within each replicate group by LC-MS/MS was quantified using label-free quantification (LFQ) and protein abundances with a sample were quantified using intensity-based absolute quantification (iBAQ) (Tyanova *et al.*, 2016). The data were analyzed by a t-test-based analysis (two valid LFQ values or more) and volcano plot analysis (three valid LFQ values). We identified 2563 and 1342 proteins in HA-IP and TurboID-based PL from the volcano plot analysis results, respectively (**Table S4**). High Pearson correlation values ($r > 0.95$) among the biological replicates of HA-IP and TurboID-based PL datasets indicate reproducibility of the data. To determine the interactors or enrichment, we used the RAW data to calculate two-sample t-tests with a permutation-based false discovery rate (FDR) of 5%. The enriched interactors of UmSee1 were designated if they had a p-value < 0.05 and log2 fold change > 1 over the control (**Fig 2A**). Finally, 262 and 67 proteins were identified by HA-IP and TurboID-based PL, respectively, and of these, 11 proteins were identified by both approaches (**Fig S1C, Table S5**). The datasets were further analyzed separately or together by psychophysiological interactions (PPIs) analysis, using the STRING database and GO (Gene Ontology) or KEGG (Kyoto Encyclopedia of Genes and Genomes) enrichment analysis using ShinyGO v0.66 (**Fig 2B-D, Fig S2, Fig S3**). PPIs and GO results suggest that the UmSee1 interactors and proteins in close proximity to UmSee1 *in planta* belong to the ubiquitin-proteasome complex.

153 **UmSee1 interacts with three UPS related proteins**

154 Based on the analysis described above, our data suggest an involvement of UmSee1
155 with proteins of the ubiquitin-proteasome system. The previously identified UmSee1-
156 interacting protein ZmSGT1 could be confirmed as an interactor in the HA-IP dataset.
157 Importantly, SGT1 is a member of the SCF (Skp1/Cullin 1/F-box) complex, which
158 associates with the ubiquitin-proteasome pathway (Cheng *et al.*, 2011). To determine
159 the specificity and relevance of our approach to identified proteins of the ubiquitin-
160 proteasome system, we chose three of the proteins identified by Co-IP and PL for
161 further analysis. We named these three proteins ZmSIPs, for *Zea mays* See1-interacting
162 protein. Zm00001eb157120 (ZmSIP1) was detected by anti-HA Co-IP and TurboID-
163 based PL, but was not significantly enriched compared to the control.
164 Zm00001eb369210 (ZmSIP2) was significantly enriched only in UmSee1 anti-HA Co-
165 IP samples and Zm00001eb185960 (ZmSIP3) was significantly enriched only in
166 TurboID-based PL datasets. Like ZmSIP2 and ZmSIP3, ZmSIP1 is also highly
167 expressed in mesophyll cells but not in the bundle sheath cells, as demonstrated by cell-
168 type specific transcriptome of maize leaves (Villajuana-Bonequi *et al.*, 2019) (**Fig S4**).
169 Furthermore, the expression of ZmSIP2 and ZmSIP3 is affected by UmSee1
170 (Villajuana-Bonequi *et al.*, 2019), which might suggest that these genes could be
171 involved in *U. maydis*-mediated tumor formation.

172 UmSee1 is localized in the nucleus and cytoplasm of plant cells (Redkar *et al.*, 2015a),
173 and we therefore tested a putative subcellular co-localization of the ZmSIPs with
174 UmSee1. The ZmSIPs were co-expressed as GFP function proteins in *N. benthamiana*
175 leaves with UmSee1-mCherry or mCherry as the control. All genes were expressed
176 under the control of the cauliflower mosaic virus (CaMV) 35S promoter. As expected,
177 fluorescence microscopy detected the mCherry signal for UmSee1 in the nucleus and
178 the cytoplasm. Similarly, GFP signals could also be detected in the nucleus and the
179 cytoplasm (**Fig S5**), suggesting that all ZmSIPs (ZmSIP1, ZmSIP2, ZmSIP3) co-
180 localize with UmSee1 in the same compartments upon co-overexpression *in planta*. To
181 test for a direct protein-protein interaction between UmSee1 and the ZmSIPs, a directed
182 yeast two-hybrid (Y2H) assay was done. The yeast transformants co-expressing each

183 of the three ZmSIP1 proteins fused N-terminally to the GAL4 activation domain
184 (pGBKT7 vector) with UmSee1, or mCherry fused N-terminally to the ADH1
185 activation domain (pGADT7 vector)) were selected on SD-Leu-Trp solid media and
186 growth in the absence of histidine (-His), which indicates physical interaction of the
187 proteins tested. In contrast to the BD-UmSee1/AD-mCherry transformants, the
188 transformants expressing either of the AD-ZmSIPs together with BD-UmSee1 at
189 OD600 < 1 (**Fig 3A**). The TurboID-based PL candidate interactor ZmSIP3 consistently
190 appeared as the interactor with the lowest affinity to UmSee1 in the Y2H assays (**Fig**
191 **3A**). Importantly, we obtained comparable results when UmSee1 was exchanged to its
192 ortholog from the maize-infecting smut species *Sporisorium reilianum*, SrSee1, in these
193 assays (**Fig. S6**). In turn, when UmSee1 was exchanged to UhSee1, the ortholog from
194 barley-infecting *Ustilago hordei*, we could not detect any growth in the absence of
195 histidine (**Fig. S6**). This is in line with the previous finding that SrSee1, but not UhSee1
196 can restore the tumor formation of the UmSee1 deletion mutant (Redkar *et al.*, 2015b).
197 We also analyzed protein-protein interactions by directed Co-IP assays. UmSee1ΔSP-
198 6HA was co-immunoprecipitated by anti-myc immunoprecipitation of ZmSIP1-4myc,
199 ZmSIP2-4myc, and ZmSIP3-4myc but not with GFP-4myc, suggesting that UmSee1
200 interacts with ZmSIP1, ZmSIP2 and ZmSIP3 *in planta* (**Fig 3B**). Again, the association
201 of ZmSIP3 and UmSee1 appeared to be the weakest, although ZmSIP2 and ZmSIP3
202 protein levels were comparable in these assays. Similarly, in split-luciferase
203 complementation imaging assays, a luminescence signal was detected when UmSee1
204 and all ZmSIPs were co-expressed in *N. benthamiana* leaves. We did not detect any
205 signal in the control samples (**Fig 3C**). Collectively, our data shows that UmSee1
206 interacts with ZmSIP1, ZmSIP2 and ZmSIP3 and that the association with ZmSIP3 may
207 be weak and/or transient interaction.
208

209 **UmSee1-interactor maize proteins are components of the ZmSGT1-complex**

210 SGT1 is known to regulate Skp1 in the SCF (Skp1/Cullin 1/F-box) complex, which
211 controls the degradation of cell cycle regulators (Hermand, 2006). UmSee1 interacts
212 with maize ZmSGT1 and can block SIPK-triggered SGT1 phosphorylation (Redkar *et*

213 *al.*, 2015a). To explore the relationship between ZmSIPs (ZmSIP1, ZmSIP2, ZmSIP3)
214 and ZmSGT1, we tested if ZmSGT1 can also associate with the here identified ZmSIPs.
215 Yeast transformants expressing BD-ZmSGT1 with AD-ZmSIP1 and AD-ZmSIP2 grew
216 on the selection medium lacking histidine. Transformants co-expressing BD-ZmSGT1
217 and AD-ZmSIP3 grew poorly in comparison, suggesting a stable association between
218 UmSGT1 and ZmSIP1 or ZmSIP2, but a weak or transient association with ZmSIP3
219 (**Fig 4A**). ZmSGT1-6HA was also co-expressed with ZmSIP1-4myc, ZmSIP2-4myc,
220 ZmSIP3-4myc or GFP-4myc in *N. benthamiana* leaves for Co-IP assays. ZmSGT1-
221 6HA was precipitated at equal levels by anti-myc immunoprecipitation of ZmSIP1-
222 4myc, ZmSIP2-4myc, and ZmSIP3-4myc but not with the GFP-4myc control (**Fig 4B**),
223 suggesting that ZmSGT1 can interplay with ZmSIP1, ZmSIP2, and ZmSIP3 *in planta.*
224

225 **UmSee1 interacts with components of the UPS to regulate cell cycle**

226 Since ZmSIP1, ZmSIP2 and ZmSIP3 are all proteins related to the ubiquitin-
227 proteasome system, we performed an activity-based protein profiling (ABPP) assay to
228 explore whether heterologous UmSee1 affects proteasome activity. For this, total
229 proteins extracted from maize leaves were mixed with or without recombinant 6His-
230 UmSee1 obtained from *E. coli*. Samples were pre-incubated in the presence or absence
231 of the proteasome inhibitor epoxomicin and labeled with the specific proteasome
232 activity-based probe MVB072 (Kolodziejek *et al.*, 2011). MVB072 binds covalently
233 and irreversible to the active site of the catalytic proteasome subunits beta-1, beta-2 and
234 beta-5 and contains a bodipy tag for fluorescent detection and a biotin tag for affinity
235 purification (Kolodziejek *et al.*, 2011). Proteasome specific signals were observed at ca.
236 26 kDa and those signals were inhibited in the presence of epoxomicin (**Fig 5A**). To
237 compare, if in the presence of See1 proteasome activity is enhanced ABPP signals were
238 quantified and percentage of activity compared to buffer was plotted. We detected
239 significantly enhanced activity of the maize proteasome in the presence of recombinant
240 6His-UmSee1ΔSP in comparison to the control sample. (**Fig 5A-B**). Thus, addition of
241 recombinant 6His-UmSee1 enhances *in-vitro* proteasome activity of maize. To explore
242 the effect of UmSee1 on the ubiquitination of maize proteins, seven-day-old maize

243 leaves were infected with *U. maydis* strains SG200 or SG200ΔSee1. Total extracted
244 proteins were detected via western blot using an α-ubiquitin antibody. We consistently
245 detected stronger ubiquitination in SG200-infected leaves when compared to
246 SG200ΔSee1-infected leaves, suggesting that UmSee1, directly or indirectly, increases
247 the ubiquitination of maize proteins during infection (**Fig 5C**). Interestingly, the
248 expression pattern of the proteasome alpha subunit ZmSIP2 is downregulated in
249 SG200ΔSee1-infected leaves in comparison to SG200 infection but the expression of
250 the catalytic beta-1 proteasome subunit PBA1 (GRMZM2G1775) does not change
251 during infection (Fig S4) (Villajuana-Bonequi *et al.*, 2019), suggesting a normal core
252 protease proteasome activity but a somehow disrupted structure of the 20S barrel in the
253 absence of UmSee1. How could one then connect UmSee1-dependent proteasomal
254 activity to its role in the activation of plant cell cycle? A possible link could be ZmSIP3,
255 which contains CDC48 and AAA+ domains related to cell cycle regulation. The protein
256 stability of ZmSIP3 may be important for cell cycle. To explore if the UmSee1-driven
257 effects on proteasome-activity and ubiquitination alter the stability of ZmSIP3, we
258 performed a protein degradation analysis of ZmSIP3 in the presence of UmSee1ΔSP-
259 mCherry-6HA, as well as an mCherry-6HA control (Fig 5D). For this, ZmSIP3-4myc,
260 mCherry-6HA and UmSee1ΔSP-mCherry-6HA were separately expressed in *N.*
261 *benthamiana* leaves using Agrobacterium-mediated transformation. ZmSIP3-4myc
262 protein extracts were supplemented with increasing concentrations of mCherry-6HA or
263 UmSee1ΔSP-mCherry-6HA-containig extracts in the presence or absence of the
264 proteasome inhibitor MG132. Samples were incubated at 28°C for 45 min, and the
265 amount of ZmSIP3-4myc was detected by western blot using anti-myc antibodies.
266 ZmSIP3-4myc protein levels decreased with increasing UmSee1ΔSP-mCherry-6HA
267 concentrations and this degradation process was reversed by the addition of MG132.
268 This decrease of ZmSIP3-4myc was significantly less seen when UmSee1ΔSP-
269 mCherry-6HA was exchanged by mCherry-6HA. These data indicate an enhanced
270 proteasome-mediated degradation of ZmSIP3 in the presence of UmSee1. Collectively,
271 our results suggest a possible UPS regulatory network modulated by UmSee1 that
272 facilitates cell cycle progression and thus promotes tumorigenesis (**Figure 5E**).

Discussion

Combination of AP-MS and PL identifies the UmSee1-interaction network

Plant pathogens target host proteins with secreted effectors to facilitate infection. Thus, the identification of effector targets helps to understand both, microbial virulence strategies, as well as mechanisms of plant immunity. Conventional approaches for identifying protein interactors are yeast-two-hybrid (Y2H) library screenings and affinity purification followed by mass spectrometry (AP-MS) (Paraoan *et al.*, 2020, Woloschuk *et al.*, 2020). ZmSGT1 was identified as an interactor of UmSee1 via a yeast-two hybrid library screen and this interaction was confirmed by AP-MS (Redkar *et al.*, 2015a). However, this strategy likely fails to explore complex effector-target interaction networks, which can be dynamic and transient in nature. Plant pathogen effectors can target multiple host proteins to effectively disrupt a single or various biological pathways and promote virulence (Khan *et al.*, 2018). For example, *Pseudomonas syringae* effector HopM1 (HopPtoM) is required for full virulence by targeting MIN7 (ARF-GEF), MIN10 (GRF10), UPL1, UPL3, and ECM29 proteins in Arabidopsis (Toruño *et al.*, 2016, Üstün *et al.*, 2016, Khan *et al.*, 2018). Another example is the effector AvrPiZ-t from *Magnaporthe oryzae,* which targets Nup98 homolog APIP12 and the E3 ligase APIP6 and APIP10 in rice to promote infection (Park *et al.*, 2012, Park *et al.*, 2016, Tang *et al.*, 2017).

Enzyme-catalyzed proximity labeling approaches have been increasingly used as an alternative screening method for capturing weak or transient protein interactions by labeling the neighboring proteins with biotin (Gingras *et al.*, 2019). TurboID-based PL is ideal for low affinity, transient interactions, and proteins insoluble under native extraction conditions (Zhang *et al.*, 2019, Melkonian *et al.*, 2022). The components of regulators and many subcellular organelles involved in various cellular processes have been identified by TurboID-based PL in mammalian cells and some model plants, but it has not been yet used in the context of fungal pathogens.

In this study, we established TurboID-based PL for exploiting the so far unidentified interactors of the organ-specific effector UmSee1 in the *U. maydis*-maize pathosystem. Combination of all putative UmSee1 interacting proteins identified by co-

303 immunoprecipitation (Co-IP) and TurboID-based PL identified components of the
304 ubiquitin-proteasome system (UPS) being enriched in the UmSee1 interaction network.
305 Three UPS-related proteins (ZmSIP1, ZmSIP2, ZmSIP3) were confirmed to interact
306 with UmSee1. ZmSIP1 contains a ubiquitin-conjugating enzyme E2 motif, catalytic
307 (UBCc) domain, suggesting that ZmSIP1 in maize may perform as a E2 ubiquitin-
308 conjugating enzyme. E2 enzymes have been found to regulate the processing and
309 topology of poly-ubiquitin chain formation and other modifications, thus, determining
310 the destiny of the modified proteins (Zhou *et al.*, 2017). The interaction of UmSee1 and
311 ZmSIP1 may be linked to the proteasome alpha subunit ZmSIP2 and the increased
312 ubiquitination observed upon *U. maydis*-infection, but the molecular mechanism
313 behind this phenotype needs to be further investigated. ZmSIP2 contains a proteasome
314 alpha type 3 domain, which is part of the central core 20S proteasome containing the
315 catalytic subunits responsible for protein degradation in the cytoplasm and nucleus. The
316 plant proteasome is a key regulator of protein stability and has been identified as a hub
317 in plant immunity since it is targeted by multiple bacterial and fungal effector molecules,
318 such as SylA and HopZ4 from *Pseudomonas syringae* or higginsianin B from the
319 fungus *Colletotrichum higginsianum* that bind and inhibit proteasome activity
320 suppressing plant immunity (Misas-Villamil *et al.*, 2013, Üstün *et al.*, 2014, Dallery *et*
321 *al.*, 2020).
322

323 **Towards an understanding of effector-mediated modulation of cell-cycle control**

324 UmSee1 interacts with and alter the function of UPS components. The observed
325 UmSee1-mediated increase in proteasome activity suggests that this effector affects
326 proteasome function or regulation, although it is not yet clear if the *in vitro* proteasomal
327 activation observed is specific for UmSee1 or if it is a consequence of UmSee1
328 degradation where UmSee1 is used as a substrate. If UmSee1 specifically activates
329 proteasomal degradation, one would expect an increased degradation efficiency of
330 certain proteins. In this context, it is important that essential cell cycle regulators are
331 associated with the UPS, and that UPS regulates cell growth and proliferation
332 boundaries between the G1 and S-phase (Bashir *et al.*, 2004). The UmSee1 interactor

333 ZmSIP3 is a CDC48 domain-containing protein, i.e. a conserved AAA+ (ATPases
334 Associated with diverse cellular Activities) ATPase, which are enzymes known to be
335 involved in cell cycle control, cytokinesis and cell proliferation (Stolz *et al.*, 2011).
336 CDC48 has been first identified in yeast, where it is important for cell cycle progression
337 (Buchberger, 2013). In plants, CDC48 is involved in multiple processes, such as
338 germination, reproduction, tissue differentiation and immune response. For example, *A.*
339 *thaliana* CDC48A is involved in embryo growth and the degradation of immune
340 receptors (Li *et al.*, 2022). Thus, the increase of UPS-mediated degradation of ZmSIP3
341 in presence of UmSee1 might provide a hint on how *U. maydis* triggers cell proliferation
342 in host. Based on our findings, a possible scenario (**Fig 5E**) is that UmSee1 interferes
343 with components of the SGT1/SCF complex to potentiate UPS activity. This leads to
344 an increased degradation of cell cycle regulators, including CDC48, which promotes
345 the activation of cell cycle progression observed in *U. maydis* induced tumorigenesis.
346 In future studies, this working model can be tested to dissect the molecular interplay
347 between the ubiquitin-proteasome system and the tumor-inducing function of UmSee1.
348 In summary, we have established TurboID-based PL in combination with Co-IP
349 followed by LC-MS/MS to identify a protein interaction network of the UmSee1
350 effector. This approach is widely applicable, in particular for establishing interaction
351 networks of effectors which interfere with complex cellular processes. Insight into
352 protein networks and their modulation by effectors will increase our mechanistic
353 understanding of microbial pathogenesis. Moreover, it provides new starting points for
354 the biochemical and structural elucidation of effector-target interactions and therefore
355 holds a strong potential to establish new strategies for plant disease control and crop
356 improvement.
357

358 **Materials and methods**

359 **Plasmid construction**

360 NEBuilder HiFi DNA Assembly (Gibson cloning method) was used for all cloning
361 processes. For the transformation of *U. maydis*, the plasmid p123-P_{Pit2}-TurboID-3HA
362 containing the native promoter of UmPit2 (UMAG_01375), TurboID and 3HA tag was

363 generated using NEBuilder HiFi DNA Assembly. This plasmid was then used to
364 generate the p123-P_{Pit2}-SP_{UmSee1}-mCherry-TurboID-3HA and the p123-P_{Pit2}-UmSee1-
365 TurboID-3HA also using NEBuilder HiFi DNA Assembly. All constructs were
366 confirmed by sequencing. For Y2H assays, cDNAs of mCherry and ZmSIPs (ZmSIP1,
367 ZmSIP2, ZmSIP3) were cloned into the pGADT7 vector (Clontech) for expression *via*
368 the GAL4 AD under constitutive ADH1 promoter. mCherry, UmSee1ΔSP, SrSee1ΔSP,
369 and UhSee1ΔSP were cloned into the pGBKT7 vector (Clontech) for expression with
370 the GAL4 DNA-BD under control of the constitutive ADH1 promoter. For CoIP and *in*
371 *vivo* protein degradation assays, cDNAs of GFP and ZmSIPs (ZmSIP1, ZmSIP2,
372 ZmSIP3) lacking stop codons were cloned into pICH47732 vector with the cauliflower
373 mosaic virus 35S promoter and a 4myc tag, CDSs of UmSee1ΔSP and ZmSGT1 were
374 cloned into pICH47732 vector with the cauliflower mosaic virus 35S promoter and a
375 6HA tag. For subcellular localization studies, ZmSIPs (ZmSIP1, ZmSIP2, ZmSIP3)
376 lacking stop codons were cloned into pICH47732 vector with the 35S promoter and a
377 GFP tag. UmSee1ΔSP was cloned into pICH47732 vector with the 35S promoter and a
378 mCherry tag. For UmSee1ΔSP protein expression in *E. coli* and subsequent ABPP,
379 UmSee1 CDS was amplified by PCR without its signal peptide and ligated into the
380 pET15b vector. All primers used are listed in **Table S1**.
381
382 **Generation of fungal strains and growth conditions**
383 *U. maydis* strains generated and used in this study are listed in **Table S2**. p123-P_{Pit2}-
384 SP_{UmSee1}-mCherry-TurboID-3HA by p123-P_{Pit2}-TurboID-3HA The p123-P_{Pit2}-
385 UmSee1-mCherry-TurboID-3HA and p123-P_{Pit2}-SP_{UmSee1}-mCherry-TurboID-3HA
386 constructs containing the carboxin resistance *ip* allele was introduced into SG200ΔSee1
387 and SG200, respectively, by homologous recombination in the *ip*-locus (Kämper, 2004)
388 All generated *U. maydis* strains were confirmed by PCR and Southern blot.
389
390 **Maize infections and biotin-treatment**
391 *U. maydis* strains were grown in liquid YEPS light medium on a shaker (200 rpm) or
392 potato dextrose agar (PD) plates at 28 °C. For assessing virulence, the seven-day-old

393 maize seedings of Early Golden Bantam (EGB) were inoculated with *U. maydis* strains
394 with an OD_{600}=1.0. Disease symptoms were scored at 12 days post-infection (dpi) as
395 described (Kämper *et al.*, 2006) and the experiment was performed at least three times
396 independently. For the preparation of samples for LC-MS/MS, seven-day-old maize
397 seedings of Early Golden Bantam (EGB) were inoculated with respective *U. maydis*
398 strains at an OD_{600}=3.0. Biotin treatment of the maize leaves was performed via
399 infiltration of a 100 μM biotin solution at two dpi.
400
401 **Sample preparation for mass spectrometry (MS)**
402 For each construct (*pPit2:SP*$_{UmSee1}$*- mCherry-TurboID -3HA*, *pPit2:UmSee1- TurboID*
403 *-3HA*), three biological replicates were performed and analyzed via MS. The biotin-
404 treated maize leaves were harvested at three days post-infection (2 days post biotin
405 treatment) and frozen in liquid nitrogen. Frozen plant material was ground to a fine
406 powder for protein extraction. These plant powders were divided into different tubes.
407 For HA-IP, the frozen powder was added to 1.5 mL ice-cold protein-lysis buffer (50
408 mM Tris pH 7.5,150 mM NaCl,10 % glycerol, 2 mM EDTA, 10 mM DTT, 0.5 %
409 IGEPAL, 1 mM PMSF) with cOmplete™ Protease Inhibitor Cocktail (Roche) and
410 incubated on ice for half an hour after vortexing. The tubes were centrifuged at 13,300
411 x g for 10 min at 4°C, the upper soluble fraction was centrifuged again at 13,300 x g
412 for 20 min at 4°C, the resulting supernatant was transferred to a fresh tube as total
413 protein extract. HA magnetic beads (Pierce Anti-HA magnetic beads, Thermo Fisher
414 Scientific) were separated on a magnetic separator. and washed three times by ice-cold
415 wash buffer (50 mM Tris–HCl pH 7.5, 150 mM NaCl, 10% glycerol, 2 mM EDTA).
416 After adding 10 μL beads to each of the cell extracts, the samples were incubated on a
417 rolling wheel at 4°C for three hours. HA magnetic beads were magnetically separated
418 and washed in 1 mL wash buffer three times. An aliquot of the beads was used for
419 immunoblotting, the antibodies used were mouse anti-HA primary antibody (1:30,000
420 dilution; Sigma-Aldrich) and anti-mouse IgG secondary antibody (1:10,000 dilution;
421 Thermo Fisher Scientific).
422 For TurboID-based PL, the frozen powder was added to 500 μl SDT-lysis buffer (10

423 mL 10% SDS, 2.5 ml 1M DTT, 2.5 mL 1M Tris pH 7.5, 10 mL ddH_2O)(Melkonian *et*
424 *al.*, 2022), and incubated 5 min at 95°C after vortex-mixing. The samples were
425 sonicated for 10 min and centrifuged for 10min at 13, 300 x g. The resulting supernatant
426 was transferred to a fresh tube as total proteins. Biotin depletion of the total proteins
427 used the methanol-chloroform-precipitation method (Melkonian *et al.*, 2022). 666 µL
428 methanol and 166 µL chloroform were added to 500 µL total protein extracts and mixed
429 with 300 µL ddH_2O. The mix was centrifuged for 10 min at 1,500 g and the supernatant
430 was discarded, the protein pellets were washed by 600 µl methanol two times and air-
431 dried for 5 min, then resuspended in 500 µL SDT-lysis buffer and incubated on
432 Eppendorf Thermomixer for 30 min at 1,250 rpm while shaking. The biotin-depleted
433 samples were diluted with PBS buffer (0.1 M phosphate, 0.15 M NaCl, pH 7.2) to a
434 final concentration of 0.5% SDS. Streptavidin-agarose beads (Thermo Fisher Scientific)
435 were washed with PBS buffer three times. After adding 50 µl beads to each sample, the
436 samples were incubated on a rolling wheel at RT for 20 h. The beads were centrifuged
437 for three min at 3500 rpm and removed the supernatant, then washed once with 2 mL
438 PBS buffer containing 2% SDS and six times with 10 mL PBS buffer. An aliquot of the
439 beads was used for immunoblotting, the antibody used was Strep-HRP (1:1,000 dilution;
440 Sigma-Aldrich).
441
442 **Identification of proteins by LC-MS**
443 Proteins from HA enrichment were submitted to an on-bead digestion. In brief, dry
444 beads were re-dissolved in 25 µL digestion buffer 1 (50 mM Tris, pH 7.5, 2M urea,
445 1mM DTT, 5 ng/µL trypsin) and incubated for 30 min at 30 °C in a Thermomixer with
446 400 rpm. Next, beads were pelleted and the supernatant was transferred to a fresh tube.
447 50 µL digestion buffer 2 (50 mM Tris, pH 7.5, 2M urea, 5 mM CAA) was added to the
448 beads, after mixing the beads were pelleted, the supernatant was collected and
449 combined with the previous one. The combined supernatants were then incubated o/n
450 at 32 °C in a Thermomixer with 400 rpm; samples were protected from light during
451 incubation. The digestion was stopped by adding 1 µL TFA and desalted with C18
452 Empore disk membranes according to the StageTip protocol (Rappsilber *et al.*, 2003).

453 For Streptavidin pulldown double amount of buffers were used (Melkonian *et al.*, 2022).
454 Dried peptides were re-dissolved in 2% ACN, 0.1% TFA (10 µL) and diluted to 0.1
455 µg/µL for analysis. Samples were analyzed using an EASY-nLC 1200 (Thermo Fisher
456 Scientific) coupled to a Q Exactive Plus mass spectrometer (Thermo Fisher Scientific).
457 Peptides were separated on 16 cm frit-less silica emitters (New Objective, 75 µm inner
458 diameter), packed in-house with reversed-phase ReproSil-Pur C18 AQ 1.9 µm resin.
459 Peptides were loaded on the column and eluted for 115 min using a segmented linear
460 gradient of 5% to 95% solvent B (0 min : 5%B; 0-5 min -> 5%B; 5-65 min -> 20%B;
461 65-90 min ->35%B; 90-100 min -> 55%; 100-105 min ->95%, 105-115 min ->95%)
462 (solvent A 0% ACN, 0.1% FA; solvent B 80% ACN, 0.1%FA) at a flow rate of 300
463 nL/min. Mass spectra were acquired in data-dependent acquisition mode with a TOP15
464 method. MS spectra were acquired in the Orbitrap analyzer with a mass range of 300–
465 1750 m/z at a resolution of 70,000 FWHM and a target value of 3×10^6 ions. Precursors
466 were selected with an isolation window of 1.3 m/z. HCD fragmentation was performed
467 at a normalized collision energy of 25. MS/MS spectra were acquired with a target value
468 of 10^5 ions at a resolution of 17,500 FWHM, a maximum injection time (max.) of 55
469 ms and a fixed first mass of m/z 100. Peptides with a charge of +1, greater than 6, or
470 with unassigned charge state were excluded from fragmentation for MS^2, dynamic
471 exclusion for 30s prevented repeated selection of precursors.
472 Raw data were processed using MaxQuant software (version 1.6.3.4,
473 http://www.maxquant.org/) with label-free quantification (LFQ) and iBAQ enabled
474 (Cox and Mann, 2008, Tyanova *et al.*, 2016). MS/MS spectra were searched by the
475 Andromeda search engine against a combined database containing the sequences from
476 Zea mays (Zm-B73-REFERENCE-NAM-5.0) from EnsemblPlants
477 (https://plants.ensembl.org/) and sequences of 248 common contaminant proteins and
478 decoy sequences. Trypsin specificity was required and a maximum of two missed
479 cleavages allowed. Minimal peptide length was set to seven amino acids.
480 Carbamidomethylation of cysteine residues was set as fixed, oxidation of methionine
481 and protein N-terminal acetylation as variable modifications. Peptide-spectrum-
482 matches and proteins were retained if they were below a false discovery rate of 1%.

483 Statistical analysis of the MaxLFQ values was carried out using Perseus (version 1.5.8.5,
484 http://www.maxquant.org/). Quantified proteins were filtered for reverse hits and hits
485 "identified by site" and MaxLFQ values were log2 transformed. After grouping samples
486 by condition only those proteins were retained for the subsequent analysis that had 2
487 valid values in one of the conditions. Two-sample t-tests were performed using a
488 permutation-based FDR of 5%. Alternatively, quantified proteins were grouped by
489 condition and only those hits were retained that had 3 valid values in one of the
490 conditions. Missing values were imputed from a normal distribution (1.8 downshift,
491 separately for each column). Volcano plots were generated in Perseus using an FDR of
492 5% and an S0=1. The Perseus output was exported and further processed using Excel.
493 Relative iBAQ values were calculated per column from MaxQuant output, scaled by a
494 factor of 10^6 and log10 transformed (Melkonian *et al.*, 2022).
495

496 **Psychophysiological interactions (PPIs) and gene ontology (GO) enrichment**
497 **analysis**

498 PPIs analysis was done by using the STRING database (https://string-db.org/)
499 (Szklarczyk *et al.*, 2021). then further analyzed by Cytoscape software (version 3.9.1,
500 https://cytoscape.org/) with CluePedia (version 1.5.9,
501 https://apps.cytoscape.org/apps/cluepedia) and ClueGo (version 2.5.9,
502 https://apps.cytoscape.org/apps/cluego) (Shannon *et al.*, 2003, Bindea *et al.*, 2009,
503 Bindea *et al.*, 2013, Mlecnik *et al.*, 2019). The GO and KEGG enrichment analysis was
504 done by ShinyGO v0.66 (http://bioinformatics.sdstate.edu/go65/) (Ge *et al.*, 2020).
505

506 **Yeast-two hybrid assay**

507 The pGBKT7 and pGADT7 plasmids were co-transformed into yeast strain AH109
508 (Clontech) using the LiCl-PEG (polyethylene glycol) method (Paiano *et al.*, 2019).
509 Yeast transformants were selected on SD-Leu-Trp plates and grown in liquid SD-Leu-
510 Trp for 16 hours before washing in ddH_2O. The cell density was adjusted to OD_{600}=1.0
511 and a dilution series was dropped out on SD-Leu-Trp and SD-Leu-Trp-His plates. Plates
512 were incubated for five days at 28°C. At least five independent clones were tested for

513 each combination.

514

515 **Agrobacterium-mediated transformation of *Nicotiana benthamiana* leaves**

516 Plasmids of interest were transformed into *Agrobacterium tumefaciens* GV3101 pmp90.
517 Single transformants were confirmed by colony PCR and grown in a liquid dYT
518 medium containing the corresponding antibiotics at 28 °C for 16 hours. Bacterial cells
519 were harvested and resuspended in infiltration buffer (10 mM MES, pH 5.6, 10 mM
520 $MgCl_2$, 200 μM acetosyringone) to a final OD_{600}=1.0. The different cultures were
521 mixed equally and then infiltrated into the leaves of four-week-old *N. benthamiana*
522 plants.

523

524 **Co-immunoprecipitation (Co-IP) and immunoblotting**

525 Leaves transformed with the constructs of interest were harvested at three days post
526 infiltration and frozen in liquid nitrogen. Frozen plant material was ground to a fine
527 powder with 1.5 mL ice-cold protein-lysis buffer (50 mM Tris pH 7.5,150 mM NaCl,10 %
528 glycerol, 2 mM EDTA, 10 mM DTT, 0.5 % IGEPAL, 1 mM PMSF) containing
529 cOmplete™ Protease Inhibitor Cocktail (Roche) for protein extraction. The protein
530 extracts were centrifuged twice, and the resulting supernatant was transferred to a fresh
531 tube as input, an aliquot of the input was used for immunoblotting. 5 μL washed Myc
532 magnetic beads (Chromotek) were added to the protein extracts of each sample and
533 samples were then incubated on a rolling wheel at 4°C. Myc magnetic beads were
534 magnetically separated and washed in 1 mL wash buffer three times. The elution
535 proteins were eluted from the beads with 2× SDS loading buffer (125 mM Tris–HCl pH
536 6.8, 20% glycerol, 4% SDS, 0.04% bromophenol blue) for immunoblotting.
537 The input or eluted proteins were separated by SDS-polyacrylamide-gel electrophoresis
538 (PAGE) gels using Gel Electrophoresis (Bio-Rad), and blotted onto polyvinylidene
539 fluoride (PVDF) membranes (Merck) using a Trans-Blot Turbo (Bio-Rad) transfer
540 system. The membranes were blocked in TBST with 3% non-fat milk. The antibodies
541 used were mouse anti-HA primary antibody (1:30,000 dilution; Sigma-Aldrich), anti-
542 mouse lgG secondary antibody (1:10,000 dilution; Thermo Fisher Scientific), rabbit

543 anti-myc primary antibody (1:5,000 dilution; Abcam) and anti-rabbit lgG secondary
544 antibody (1:3,000 dilution; Cell Signaling). The membranes were probed with primary
545 antibody for two hours or overnight and secondary antibody for one hour. TBST washed
546 membranes were detected with the SuperSignal luminol-based chemiluminescent
547 substrate (Thermo Fisher Scientific) by the CCD imaging system (ChemiDoc, Bio-
548 RAD).
549

550 **Split-luciferase complementation (split-LUC) assay**

551 Split-LUC assays in *N. benthamiana* were performed as described (Zhou *et al.*, 2018).
552 Agrobacterium-mediated transformation of *N. benthamiana* leaves was performed as
553 described above. For luciferase measurements, leaves were harvested two days post-
554 infiltration and sprayed with 1 mM D-luciferin for 10 min in the dark. The luminescence
555 signals of the leaves from three independent plants were detected by the CCD imaging
556 system (ChemiDoc, Bio-RAD).
557

558 **Purification of Umsee1 and Activity-based protein profiling (ABPP)**

559 The pET15b-UmSee1ΔSP plasmid was transformed into Rosetta (DE3) competent cells
560 and recombinant protein expression was initiated by 0.1 mM IPTG treatment at OD_{600}=
561 0.6-0.8. Then cells were incubated at 18°C shaking at 120 rpm for 18 h. Cells were
562 harvested and lysed using a microfluidizer. 6His-UmSee1ΔSP protein was purified
563 using affinity chromatography with Ni-NTA column (Thermo Fisher Scientific) and
564 further purified using size exclusion chromatography with HiLoad Superdex 75 16/600
565 column (GE-Healthcare) (Li and Sousa, 2012). The ABPP assays were performed as
566 described before (Kolodziejek *et al.*, 2011, Misas-Villamil *et al.*, 2017). In brief, maize
567 leaves were ground and resuspended in 50 mM Tris-HCl buffer (pH 7). The supernatant
568 was pre-incubated for 30 minutes with or without 5 μM (final concentration)
569 recombinant 6His-UmSee1ΔSP or with 20 μM (final concentration) Epoxomicin or
570 DMSO. Then, samples were incubated with 1 μM (final concentration) of the
571 proteasome probe MVB072 for 2 h. Samples were denatured at 95°C in 2x SDS loading
572 buffer and separated on SDS-PAGE gels. The probe was detected using the rhodamine

filter (excitation: 532 nm, emission: 580 nm) on a ChemiDoc (Bio-Rad). The gel was stained with SyproRuby (Invitrogen) to determine equal loading according to the manufacturer's instructions. Quantification of the signals was performed by Image J (Schneider *et al.*, 2012), all the images were transformed into gray-scale and 8-bit type for further analysis. The intensity was normalized to the loading control first, then the final signals were normalized to the epoxomicin control.

Protein degradation assay

Protein degradation assays were performed as described before (Liu *et al.*, 2010). In brief *N. benthamiana* leaves expressing mCherry-6HA UmSee1ΔSP-mCherry-6HA and ZmSIP3-4myc proteins were harvested three days post-infiltration and frozen in liquid nitrogen. Frozen plant material was ground to a fine powder with 1.0 mL ice-cold lysis buffer (250 mM Tris pH 7.5,150 mM NaCl, 10 % glycerol) for protein extraction. The protein extracts were centrifuged twice at 13,000 x g for 20 min, and the resulting supernatant was transferred to a fresh tube. ZmSIP3-4myc protein extracts were mixed in different proportions with mCherry-6HA or UmSee1ΔSP-mCherry-6HA protein extracts and treated with 100 μM (final concentration) proteasome inhibitor MG132 or DMSO for 45 minutes at 28 °C. The reactions were stopped by boiling samples at 95°C in 2x SDS loading buffer for 10 min, and separated on SDS-PAGE gels. Samples were analyzed by western blot using anti-myc and anti-HA at concentrations specified above. The membrane was stained with Coomassie brilliant blue (CBB) to determine equal protein loading.

Subcellular localization assay

At three days post-transformation of *N. benthamiana* leaves, fluorescent signals were analyzed using a Leica TCS SP8 confocal laser scanning microscope (Leica) using filters for GFP (excitation 458 nm and emission 470-490 nm) and mCherry (excitation 561 nm and emission 590-603 nm).

603 **Acknowledgments**

604 We would like to thank Weiliang Zuo for the helpful discussion and suggestions, Ute
605 Meyer for the technical support, Anne Harzen for MS sample processing, Katharina
606 Melkonian for helpful practical advice on the TurboID PL approach and Hermen
607 Overkleeft for proving the MVB072 probe. GD; JCMV and IS acknowledge support
608 from the Cluster of Excellence on Plant Sciences (CEPLAS) funded by the Deutsche
609 Forschungsgemeinschaft (DFG, German Research Foundation) under Germany's
610 Excellence Strategy – EXC 2048/1 – Project ID: 390686111. This work was funded by
611 the European Research Council under the European Union's Horizon 2020 research
612 and innovation program (consolidator grant conVIRgens, ID 771035) to GD, the DFG
613 Emmy Noether Programme (SA 4093/1-1) to IMLS and the Daimler and Benz
614 Foundation (to IMLS). HN is supported by the Max Planck Society and is grateful for
615 funding by the DFG (NA 946/1-1).

616

617 **Author contributions**

618 W.S., I.M.L.S. J.C.M.V., and G.D. designed the research. W.S., S.C.S., H.N., J.C.M.V.,
619 I.M.L.S. and G.D. performed the experiments and data analysis. W.S., J.C.M.V.,
620 I.M.L.S. and G.D. wrote the paper with contributions from all the other authors.

621

622 **References**

623 **Bashir, T., Dorrello, N.V., Amador, V., Guardavaccaro, D. and Pagano, M.** (2004)
624 Control of the SCFSkp2–Cks1 ubiquitin ligase by the APC/CCdh1 ubiquitin
625 ligase. *Nature*, **428**, 190-193.

626 **Bindea, G., Galon, J. and Mlecnik, B.** (2013) CluePedia Cytoscape plugin: pathway
627 insights using integrated experimental and in silico data. *Bioinformatics*, **29**,
628 661-663.

629 **Bindea, G., Mlecnik, B., Hackl, H., Charoentong, P., Tosolini, M., Kirilovsky, A.,**
630 **Fridman, W.H., Pages, F., Trajanoski, Z. and Galon, J.** (2009) ClueGO: a
631 Cytoscape plug-in to decipher functionally grouped gene ontology and pathway
632 annotation networks. *Bioinformatics*, **25**, 1091-1093.

633 **Bindics, J., Khan, M., Uhse, S., Kogelmann, B., Baggely, L., Reumann, D., Ingole,**
634 **K.D., Stirnberg, A., Rybecky, A., Darino, M., Navarrete, F., Doehlemann,**
635 **G. and Djamei, A.** (2022) Many ways to TOPLESS - manipulation of plant
636 auxin signalling by a cluster of fungal effectors. *New Phytol*, **236**, 1455-1470.
637 **Branon, T.C., Bosch, J.A., Sanchez, A.D., Udeshi, N.D., Svinkina, T., Carr, S.A.,**
638 **Feldman, J.L., Perrimon, N. and Ting, A.Y.** (2018) Efficient proximity
639 labeling in living cells and organisms with TurboID. *Nat Biotechnol*, **36**, 880-
640 887.
641 **Buchberger, A.** (2013) Roles of Cdc48 in regulated protein degradation in yeast.
642 *Subcell Biochem*, **66**, 195-222.
643 **Cheng, Y.T., Li, Y.Z., Huang, S.A., Huang, Y., Dong, X.N., Zhang, Y.L. and Li, X.**
644 (2011) Stability of plant immune-receptor resistance proteins is controlled by
645 SKP1-CULLIN1-F-box (SCF)-mediated protein degradation. *P Natl Acad Sci*
646 *USA*, **108**, 14694-14699.
647 **Conlan, B., Stoll, T., Gorman, J.J., Saur, I. and Rathjen, J.P.** (2018) Development
648 of a rapid in planta BioID system as a probe for plasma membrane-associated
649 immunity proteins. *Frontiers in Plant Science*, **9**, 1882.
650 **Cox, J. and Mann, M.** (2008) MaxQuant enables high peptide identification rates,
651 individualized ppb-range mass accuracies and proteome-wide protein
652 quantification. *Nature biotechnology*, **26**, 1367-1372.
653 **Dallery, J.F., Zimmer, M., Halder, V., Suliman, M., Pigne, S., Le Goff, G., Gianniou,**
654 **D.D., Trougakos, I.P., Ouazzani, J., Gasperini, D. and O'Connell, R.J.** (2020)
655 Inhibition of jasmonate-mediated plant defences by the fungal metabolite
656 higginsianin B. *J Exp Bot*, **71**, 2910-2921.
657 **Dang, F., Nie, L. and Wei, W.** (2021) Ubiquitin signaling in cell cycle control and
658 tumorigenesis. *Cell Death Differ*, **28**, 427-438.
659 **Darino, M., Chia, K.S., Marques, J., Aleksza, D., Soto-Jimenez, L.M., Saado, I.,**
660 **Uhse, S., Borg, M., Betz, R., Bindics, J., Zienkiewicz, K., Feussner, I., Petit-**
661 **Houdenot, Y. and Djamei, A.** (2021) *Ustilago maydis* effector Jsi1 interacts
662 with Topless corepressor, hijacking plant jasmonate/ethylene signaling. *New*

663 *Phytol*, **229**, 3393-3407.
664 **Dielen, A.S., Badaoui, S., Candresse, T. and GERMAN-RETANA, S.** (2010) The
665 ubiquitin/26S proteasome system in plant–pathogen interactions: a never-
666 ending hide-and-seek game. *Molecular plant pathology*, **11**, 293-308.
667 **Djamei, A., Schipper, K., Rabe, F., Ghosh, A., Vincon, V., Kahnt, J., Osorio, S.,**
668 **Tohge, T., Fernie, A.R., Feussner, I., Feussner, K., Meinicke, P., Stierhof,**
669 **Y.D., Schwarz, H., Macek, B., Mann, M. and Kahmann, R.** (2011) Metabolic
670 priming by a secreted fungal effector. *Nature*, **478**, 395-398.
671 **Dodds, P.N. and Rathjen, J.P.** (2010) Plant immunity: towards an integrated view of
672 plant-pathogen interactions. *Nat Rev Genet*, **11**, 539-548.
673 **Doehlemann, G., Reissmann, S., Aßmann, D., Fleckenstein, M. and Kahmann, R.**
674 (2011) Two linked genes encoding a secreted effector and a membrane protein
675 are essential for *Ustilago maydis*-induced tumour formation. *Molecular*
676 *microbiology*, **81**, 751-766.
677 **Doehlemann, G., van der Linde, K., Amann, D., Schwammbach, D., Hof, A.,**
678 **Mohanty, A., Jackson, D. and Kahmann, R.** (2009) Pep1, a secreted effector
679 protein of *Ustilago maydis*, is required for successful invasion of plant cells.
680 *Plos Pathogens*, **5**, e1000290.
681 **Doehlemann, G., Wahl, R., Horst, R.J., Voll, L.M., Usadel, B., Poree, F., Stitt, M.,**
682 **Pons-Kuhnemann, J., Sonnewald, U., Kahmann, R. and Kamper, J.** (2008)
683 Reprogramming a maize plant: transcriptional and metabolic changes induced
684 by the fungal biotroph *Ustilago maydis*. *Plant J*, **56**, 181-195.
685 **Fisher, M.C., Gow, N.A. and Gurr, S.J.** (2016) Tackling emerging fungal threats to
686 animal health, food security and ecosystem resilience. *Philos Trans R Soc Lond*
687 *B Biol Sci*, **371**.
688 **Ge, S.X., Jung, D. and Yao, R.** (2020) ShinyGO: a graphical gene-set enrichment tool
689 for animals and plants. *Bioinformatics*, **36**, 2628-2629.
690 **Gingras, A.C., Abe, K.T. and Raught, B.** (2019) Getting to know the neighborhood:
691 using proximity-dependent biotinylation to characterize protein complexes and
692 map organelles. *Curr Opin Chem Biol*, **48**, 44-54.

693 **Hermand, D.** (2006) F-box proteins: more than baits for the SCF? *Cell Division*, **1**, 1-
694 6.
695 **Hogenhout, S.A., Van der Hoorn, R.A.L., Terauchi, R. and Kamoun, S.** (2009)
696 Emerging concepts in effector biology of plant-associated organisms. *Mol Plant*
697 *Microbe In*, **22**, 115-122.
698 **Holzer, E., Rumpf-Kienzl, C., Falk, S. and Dammermann, A.** (2022) A modified
699 TurboID approach identifies tissue-specific centriolar components in *C. elegans*.
700 *PLoS Genet*, **18**, e1010150.
701 **Jacobs, C., Domian, I.J., Maddock, J.R. and Shapiro, L.** (1999) Cell cycle-
702 dependent polar localization of an essential bacterial histidine kinase that
703 controls DNA replication and cell division. *Cell*, **97**, 111-120.
704 **Kahmann, R. and Kamper, J.** (2004) *Ustilago maydis*: how its biology relates to
705 pathogenic development. *New Phytologist*, **164**, 31-42.
706 **Kämper, J.** (2004) A PCR-based system for highly efficient generation of gene
707 replacement mutants in *Ustilago maydis*. *Molecular genetics and genomics*, **271**,
708 103-110.
709 **Kämper, J., Kahmann, R., Bölker, M., Ma, L.-J., Brefort, T., Saville, B.J., Banuett,**
710 **F., Kronstad, J.W., Gold, S.E. and Müller, O.** (2006) Insights from the
711 genome of the biotrophic fungal plant pathogen *Ustilago maydis*. *Nature*, **444**,
712 97-101.
713 **Khan, M., Seto, D., Subramaniam, R. and Desveaux, D.** (2018) Oh, the places they'll
714 go! A survey of phytopathogen effectors and their host targets. *Plant Journal*,
715 **93**, 651-663.
716 **Kitagawa, K., Skowyra, D., Elledge, S.J., Harper, J.W. and Hieter, P.** (1999) SGT1
717 encodes an essential component of the yeast kinetochore assembly pathway and
718 a novel subunit of the SCF ubiquitin ligase complex. *Mol Cell*, **4**, 21-33.
719 **Kolodziejek, I., Misas-Villamil, J.C., Kaschani, F., Clerc, J., Gu, C., Krahn, D.,**
720 **Niessen, S., Verdoes, M., Willems, L.I., Overkleeft, H.S., Kaiser, M. and van**
721 **der Hoorn, R.A.** (2011) Proteasome activity imaging and profiling
722 characterizes bacterial effector syringolin A. *Plant Physiol*, **155**, 477-489.

723 **Lanver, D., Tollot, M., Schweizer, G., Lo Presti, L., Reissmann, S., Ma, L.S.,**
724 **Schuster, M., Tanaka, S., Liang, L., Ludwig, N. and Kahmann, R.** (2017)
725 *Ustilago maydis* effectors and their impact on virulence. *Nature Reviews*
726 *Microbiology*, **15**, 409-421.
727 **Larochelle, M., Bergeron, D., Arcand, B. and Bachand, F.** (2019) Proximity-
728 dependent biotinylation mediated by TurboID to identify protein-protein
729 interaction networks in yeast. *Journal of Cell Science*, **132**, jcs232249.
730 **Li, J., Yuan, J., Li, Y., Sun, H., Ma, T., Huai, J., Yang, W., Zhang, W. and Lin, R.**
731 (2022) The CDC48 complex mediates ubiquitin-dependent degradation of intra-
732 chloroplast proteins in plants. *Cell Rep*, **39**, 110664.
733 **Li, Y. and Sousa, R.** (2012) Expression and purification of *E. coli* BirA biotin ligase
734 for in vitro biotinylation. *Protein Expr Purif*, **82**, 162-167.
735 **Liu, L., Zhang, Y., Tang, S., Zhao, Q., Zhang, Z., Zhang, H., Dong, L., Guo, H. and**
736 **Xie, Q.** (2010) An efficient system to detect protein ubiquitination by
737 agroinfiltration in *Nicotiana benthamiana*. *Plant J*, **61**, 893-903.
738 **Mair, A., Xu, S.L., Branon, T.C., Ting, A.Y. and Bergmann, D.C.** (2019) Proximity
739 labeling of protein complexes and cell-type-specific organellar proteomes in
740 Arabidopsis enabled by TurboID. *Elife*, **8**, e47864.
741 **Matei, A., Ernst, C., Günl, M., Thiele, B., Altmüller, J., Walbot, V., Usadel, B. and**
742 **Doehlemann, G.** (2018) How to make a tumour: cell type specific dissection of
743 *Ustilago maydis*-induced tumour development in maize leaves. *New Phytologist*,
744 **217**, 1681-1695.
745 **Melkonian, K., Stolze, S.C., Harzen, A. and Nakagami, H.** (2022) miniTurbo-based
746 interactomics of two plasma membrane-localized SNARE proteins in
747 *Marchantia polymorpha*. *New Phytol*, **235**, 786-800.
748 **Misas-Villamil, J.C., Kolodziejek, I., Crabill, E., Kaschani, F., Niessen, S., Shindo,**
749 **T., Kaiser, M., Alfano, J.R. and van der Hoorn, R.A.** (2013) *Pseudomonas*
750 *syringae* pv. syringae uses proteasome inhibitor syringolin A to colonize from
751 wound infection sites. *PLoS Pathog*, **9**, e1003281.
752 **Misas-Villamil, J.C., van der Burgh, A.M., Grosse-Holz, F., Bach-Pages, M.,**

753 **Kovacs, J., Kaschani, F., Schilasky, S., Emon, A.E., Ruben, M., Kaiser, M.,**
754 **Overkleeft, H.S. and van der Hoorn, R.A.** (2017) Subunit-selective
755 proteasome activity profiling uncovers uncoupled proteasome subunit activities
756 during bacterial infections. *Plant J*, **90**, 418-430.
757 **Misas Villamil, J.C., Mueller, A.N., Demir, F., Meyer, U., Ökmen, B., Schulze**
758 **Hüynck, J., Breuer, M., Dauben, H., Win, J. and Huesgen, P.F.** (2019) A
759 fungal substrate mimicking molecule suppresses plant immunity via an inter-
760 kingdom conserved motif. *Nature communications*, **10**, 1-15.
761 **Mlecnik, B., Galon, J. and Bindea, G.** (2019) Automated exploration of gene ontology
762 term and pathway networks with ClueGO-REST. *Bioinformatics*, **35**, 3864-
763 3866.
764 **Mueller, A.N., Ziemann, S., Treitschke, S., Assmann, D. and Doehlemann, G.** (2013)
765 Compatibility in the *Ustilago maydis*-maize interaction requires inhibition of
766 host cysteine proteases by the fungal effector Pit2. *Plos Pathogens*, **9**, e1003177.
767 **Navarrete, F., Grujic, N., Stirnberg, A., Saado, I., Aleksza, D., Gallei, M., Adi, H.,**
768 **Alcantara, A., Khan, M., Bindics, J., Trujillo, M. and Djamei, A.** (2021) The
769 Pleiades are a cluster of fungal effectors that inhibit host defenses. *Plos*
770 *Pathogens*, **17**, e1009641.
771 **Ngounou Wetie, A.G., Sokolowska, I., Woods, A.G., Roy, U., Deinhardt, K. and**
772 **Darie, C.C.** (2014) Protein–protein interactions: switch from classical methods
773 to proteomics and bioinformatics-based approaches. *Cellular and molecular life*
774 *sciences*, **71**, 205-228.
775 **Paiano, A., Margiotta, A., De Luca, M. and Bucci, C.** (2019) Yeast two-hybrid assay
776 to identify interacting proteins. *Curr Protoc Protein Sci*, **95**, e70.
777 **Paraoan, L.I., Sharif, U., Kelly, L. and Carlsson, E.** (2020) Intracellular RPE
778 interactome analysis of protein variants associated with AMD by affinity
779 purification mass spectrometry. *Invest Ophth Vis Sci*, **61**.
780 **Park, C.H., Chen, S.B., Shirsekar, G., Zhou, B., Khang, C.H., Songkumarn, P.,**
781 **Afzal, A.J., Ning, Y.S., Wang, R.Y., Bellizzi, M., Valent, B. and Wang, G.L.**
782 (2012) The *Magnaporthe oryzae* effector AvrPiz-t targets the RING E3

783 ubiquitin ligase APIP6 to suppress pathogen-associated molecular pattern-
784 triggered Immunity in Rice. *Plant Cell*, **24**, 4748-4762.
785 **Park, C.H., Shirsekar, G., Bellizzi, M., Chen, S., Songkumarn, P., Xie, X., Shi, X.,**
786 **Ning, Y., Zhou, B., Suttiviriya, P., Wang, M., Umemura, K. and Wang, G.L.**
787 (2016) The E3 ligase APIP10 connects the effector AvrPiz-t to the NLR receptor
788 Piz-t in rice. *PLoS Pathog*, **12**, e1005529.
789 **Rappsilber, J., Ishihama, Y. and Mann, M.** (2003) Stop and go extraction tips for
790 matrix-assisted laser desorption/ionization, nanoelectrospray, and LC/MS
791 sample pretreatment in proteomics. *Anal Chem*, **75**, 663-670.
792 **Redkar, A., Hoser, R., Schilling, L., Zechmann, B., Krzymowska, M., Walbot, V.**
793 **and Doehlemann, G.** (2015a) A secreted effector protein of *Ustilago maydis*
794 guides maize leaf cells to form tumors. *Plant Cell*, **27**, 1332-1351.
795 **Redkar, A., Villajuana-Bonequi, M. and Doehlemann, G.** (2015b) Conservation of
796 the *Ustilago maydis* effector See1 in related smuts. *Plant Signal Behav*, **10**,
797 e1086855.
798 **Saado, I., Chia, K.S., Betz, R., Alcantara, A., Pettko-Szandtner, A., Navarrete, F.,**
799 **D'Auria, J.C., Kolomiets, M.V., Melzer, M., Feussner, I. and Djamei, A.**
800 (2022) Effector-mediated relocalization of a maize lipoxygenase protein
801 triggers susceptibility to *Ustilago maydis*. *Plant Cell*, **34**, 2785-2805.
802 **Schneider, C.A., Rasband, W.S. and Eliceiri, K.W.** (2012) NIH Image to ImageJ: 25
803 years of image analysis. *Nat Methods*, **9**, 671-675.
804 **Sciuto, M.R., Coppola, V., Iannolo, G., De Maria, R. and Haas, T.L.** (2019) Two-
805 Step Co-Immunoprecipitation (TIP). *Curr Protoc Mol Biol*, **125**, e80.
806 **Shannon, P., Markiel, A., Ozier, O., Baliga, N.S., Wang, J.T., Ramage, D., Amin,**
807 **N., Schwikowski, B. and Ideker, T.** (2003) Cytoscape: a software environment
808 for integrated models of biomolecular interaction networks. *Genome Res*, **13**,
809 2498-2504.
810 **Skibbe, D.S., Doehlemann, G., Fernandes, J. and Walbot, V.** (2010) Maize tumors
811 caused by *Ustilago maydis* require organ-specific genes in host and pathogen.
812 *Science*, **328**, 89-92.

Stolz, A., Hilt, W., Buchberger, A. and Wolf, D.H. (2011) Cdc48: a power machine in protein degradation. *Trends Biochem Sci*, **36**, 515-523.

Szklarczyk, D., Gable, A.L., Nastou, K.C., Lyon, D., Kirsch, R., Pyysalo, S., Doncheva, N.T., Legeay, M., Fang, T., Bork, P., Jensen, L.J. and von Mering, C. (2021) The STRING database in 2021: customizable protein-protein networks, and functional characterization of user-uploaded gene/measurement sets. *Nucleic Acids Res*, **49**, D605-D612.

Tanaka, S., Brefort, T., Neidig, N., Djamei, A., Kahnt, J., Vermerris, W., Koenig, S., Feussner, K., Feussner, I. and Kahmann, R. (2014) A secreted *Ustilago maydis* effector promotes virulence by targeting anthocyanin biosynthesis in maize. *Elife*, **3**, e01355.

Tang, M.Z., Ning, Y.S., Shu, X.L., Dong, B., Zhang, H.Y., Wu, D.X., Wang, H., Wang, G.L. and Zhou, B. (2017) The Nup98 homolog APIP12 targeted by the effector AvrPiz-t is involved in rice basal resistance against *Magnaporthe oryzae*. *Rice*, **10**, 1-11.

Toruño, T.Y., Stergiopoulos, I. and Coaker, G. (2016) Plant-pathogen effectors: cellular probes interfering with plant defenses in spatial and temporal manners. *Annual review of phytopathology*, **54**, 419.

Tyanova, S., Temu, T. and Cox, J. (2016) The MaxQuant computational platform for mass spectrometry-based shotgun proteomics. *Nature protocols*, **11**, 2301-2319.

Üstün, S., König, P., Guttman, D.S. and Börnke, F. (2014) HopZ4 from *Pseudomonas syringae*, a member of the HopZ type III effector family from the YopJ superfamily, inhibits the proteasome in plants. *Mol Plant Microbe In*, **27**, 611-623.

Üstün, S., Sheikh, A., Gimenez-Ibanez, S., Jones, A., Ntoukakis, V. and Börnke, F. (2016) The proteasome acts as a hub for plant immunity and is targeted by Pseudomonas type III effectors. *Plant physiology*, **172**, 1941-1958.

Villajuana-Bonequi, M., Matei, A., Ernst, C., Hallab, A., Usadel, B. and Doehlemann, G. (2019) Cell type specific transcriptional reprogramming of maize leaves during *Ustilago maydis* induced tumor formation. *Sci Rep*, **9**,

843 10227.
844 **Woloschuk, R.M., Reed, P.M.M., McDonald, S., Uppalapati, M. and Woolley, G.A.**
845 (2020) Yeast two-hybrid screening of photoswitchable protein-protein
846 interaction libraries. *J Mol Biol*, **432**, 3113-3126.
847 **Zhang, Y.L., Song, G.Y., Lai, N.K., Nagalakshmi, U., Li, Y.Y., Zheng, W.J., Huang,**
848 **P.J., Branon, T.C., Ting, A.Y., Walley, J.W. and Dinesh-Kumar, S.P.** (2019)
849 TurboID-based proximity labeling reveals that UBR7 is a regulator of N NLR
850 immune receptor-mediated immunity. *Nature Communications*, **10**, 1-17.
851 **Zhou, B.J., Mural, R.V., Chen, X.Y., Oates, M.E., Connor, R.A., Martin, G.B.,**
852 **Gough, J.L. and Zeng, L.R.** (2017) A subset of ubiquitin-conjugating enzymes
853 is essential for plant immunity. *Plant Physiology*, **173**, 1371-1390.
854 **Zhou, Z., Bi, G. and Zhou, J.M.** (2018) Luciferase complementation assay for protein-
855 protein interactions in p lants. *Curr Protoc Plant Biol*, **3**, 42-50.
856

857 **Figure legends**

858 **Fig 1.: Experimental setup for TurboID-based biotin labeling in the *Ustilago*-maize**
859 **system.**

860 (**A**) Principle to isolate further UmSee1-interacting proteins and proteins in close
861 proximity to UmSee1 in maize leaves *vi*a Pull-down and TurboID-based proximity
862 labelling (PL). (**B**) Schematic representation of the constructs used for HA-IP and
863 Turbo-based PL. (**C**) Quantification of infection symptoms on EGB maize seedlings
864 infected with *U. maydis* strains as indicated in B at 12 dpi. SG200: wild-type *U. maydis*,
865 mCherry-TurboID-HA/SG200: mCherry-TurboID-3HA expressed in wild-type *U.*
866 *maydis*, ΔSee1: *See1* deletion mutant, UmSee1-TurboID-3HA/ΔSee1: UmSee1-
867 TurboID-3HA expressed in *See1* deletion mutant. (**D**) Detection of mCherry-TurboID-
868 HA and UmSee1-TurboID-HA in maize leaves upon delivery by *U. maydis.* For anti-
869 HA immunoprecipitation, leaves were harvested at three days post infection. Three
870 independent replicates (Rep1-3) are shown. M: protein ladder. The asterisks represent
871 target proteins. Expected size of mCherry-TurboID-3HA and UmSee1-TurboID-3HA
872 proteins are 68.0 and 54.5 kDa, respectively. (**E**) Overview of the workflow used to
873 identify putative UmSee1 targets by Co-Immunoprecipitation (Co-IP) and TurboID-
874 based biotin labeling in the *Ustilago maydis*-maize pathosystem.

875

876 **Fig 2.: Identification of UmSee1 interacting proteins by co-immunoprecipitation**
877 **(Co-IP) and TurboID-based biotin labeling.**

878 (**A**) Volcano plot analysis of identified proteins from HA-IP and TurboID-based biotin
879 labeling by LC-MS/MS. Proteins significantly enriched in UmSee1 samples are shown
880 in the top right corner (red and yellow dots). HA-up (yellow dots): significantly
881 enriched proteins in UmSee1 compared to mCherry samples in the HA pull-down; HA-
882 down (blue dots): significantly enriched proteins in mCherry compared to UmSee1
883 samples in the HA pull-down, HA-No (green dots): no significantly enriched proteins
884 between UmSee1 and mCherry-samples in HA pull-down dataset, Turbo-up (red
885 triangle): significantly enriched proteins in UmSee1 compared to mCherry samples in
886 the TurboID-based proximity labeling; Turbo-down (purple triangles): significantly

887 enriched proteins in mCherry compared to UmSee1 samples in the TurboID-based
888 proximity labeling, Turbo-No (green triangles): no significantly enriched proteins
889 between UmSee1 and mCherry samples in the TurboID-based proximity labeling
890 dataset. (p-value < 0.05 and log2 fold change > 1 set as significantly enriched). (**B**)
891 Protein-Protein interaction (PPI) analysis of the proteins identified in UmSee1 samples
892 using the STRING database. Proteins significantly enriched in the HA-IP and TurboID-
893 based PL of UmSee1 samples were submitted to the STRING database, and the protein
894 interaction network was modified and analyzed using the Cytoscape software (version
895 3.9.1). Edges represent protein-protein associations, including known interactions and
896 predicted interactions (gene neighbourhood, gene fusions, gene co-occurrence), the
897 identified protein by the different methods were marked with different colors, and the
898 shape's size indicates the degree of interaction. Proteins are represented by their gene
899 ID. (**C**) Cluster analysis of the Protein-Protein interactions network of the UmSee1-
900 specific dataset by CluePedia (version 1.5.9) and ClueGo (version 2.5.9). (**D**) Gene
901 Ontology (GO) cellular component enrichment of the UmSee1-specific dataset using
902 ShinyGO v0.66.
903
904 **Fig 3.: Three identified proteins enriched in theUmSee1 dataset interact with**
905 **UmSee1 in one-to-one interaction assays.**
906 (**A**) Y2H assay of UmSee1 and three putative UmSee1 interaction partners (ZmSIPs).
907 The yeast strain AH109 was co-transformed with mCherry or UmSee1ΔSP (UmSee1
908 without signal peptide) and the constructs of ZmSIPs (ZmSIP1, ZmSIP2, ZmSIP3). A
909 drop-out assay of dilution series of the double-transformants was made in the presence
910 (SD-Trp-Leu) and absence (SD-Trp-Leu-His) of histidine. Yeast growth in the absence
911 of histidine suggests the interaction of proteins. Pictures of three independent
912 experiments were taken 5 days after plating (**B**) Co-Immunoprecipitation assays of
913 UmSee1 and the three ZmSIPs. *N. benthamiana* leaves were transiently transformed
914 with the constructs encoding UmSee1ΔSP-6HA and ZmSIPs-4myc or GFP-4Myc.
915 Leaves were harvested three days post-Agrobacterium-mediated transformation for
916 protein extraction. Anti-myc immunoprecipitation (IP) was performed and total extracts

917 and IP proteins were detected by western blot analysis using anti-HA and anti-myc.
918 Expected size of GFP-4myc, ZmSIP1-4myc, ZmSIP2-4myc, ZmSIP3-4myc and
919 UmSee1ΔSP-6HA proteins are 31.9, 20.5, 32.2, 86.1 and 26.4 kDa, respectively. (**C**)
920 Split-luciferase assay of UmSee1 and the three ZmSIPs. *N. benthamiana* plants were
921 transiently transformed with constructs of UmSee1ΔSP-nLUC or mCherry-nLUC and
922 cLUC-ZmSIPs (ZmSIP1, ZmSIP2, ZmSIP3) or cLUC as indicated. Leaves were
923 harvested two days post Agrobacterium-mediated transformation and treated with 1
924 mM D-luciferin for 10 min in the dark. Shown are representative pictures of
925 luminescence signals from three independent biological replicates. Images were
926 detected by the CCD imaging system (ChemiDoc, Bio-RAD).
927
928 **Fig 4.: Three identified UmSee1-interactors are associated with the ZmSGT1-**
929 **interacting protein complex.**
930 (**A**) Y2H assays of SGT1 and the three ZmSIPs. The yeast strain AH109 was co-
931 transformed with ZmSGT1 and the three ZmSIPs, ZmSIP1, ZmSIP2, ZmSIP3, or
932 mCherry as a negative control. A drop-out assay of dilution series of the double-
933 transformants was made in the presence (SD-Trp-Leu) and absence (SD-Trp-Leu-His)
934 of histidine. Yeast growth in the absence of histidine suggests the interaction of proteins.
935 Shown are representative pictures of three independent biological experiments taken 5
936 days after drop out plating. (**B**) Co-Immunoprecipitation assays of ZmSGT1 and the
937 ZmSIPs. *N. benthamiana* leaves were transiently transformed with the ZmSGT1-6HA
938 and ZmSIPs (ZmSIP1, ZmSIP2, ZmSIP3)-4myc constructs. Leaves were harvested
939 three days post-Agrobacterium-mediated transformation for protein extraction. Anti-
940 myc immunoprecipitation (IP) was performed and total extracts and IP proteins were
941 detected by western blot analysis using anti-HA and anti-myc. Expected size of GFP-
942 4myc, ZmSIP1-4myc, ZmSIP2-4myc, ZmSIP3-4myc and ZmSGT1-6HA proteins are
943 31.9, 20.5, 32.2, 86.1 and 53.6 kDa, respectively.
944
945 **Fig 5.: UmSee1 enhances proteasome activity and can promote ZmSIP3**
946 **degradation.**

947 (**A**) Activity-based protein profiling (ABPP) of the effect of recombinant UmSee1 on
948 proteasome activity. Total proteins extracted from maize leaves were mixed with the
949 probe MVB072. Samples were pre-incubated with or without recombinant
950 UmSee1_His and with or without the proteasome inhibitor epoxomicin. Samples were
951 analyzed by gel electrophoresis and monitored using a Rhodamine filter. SyproRuby
952 staining served as loading control. Purified 6His-UmSee1ΔSP were detected by western
953 blot using an anti-His antibody. (**B**) Relative proteasome activity quantification of (A).
954 (**C**) Maize ubiquitin activity upon infection with *U. maydis* strains SG200 and
955 SG200ΔSee1. Leaves were harvested three days post-infection and total protein
956 extracts were analyzed by anti-ubiquitin western blot. SyproRuby staining serves as
957 loading control. (**D**) In vitro protein degradation analysis of ZmSIP3. ZmSIP3-4myc,
958 mCherry-6HA and UmSee1ΔSP-mCherry-6HA were separately expressed in *N.*
959 *benthamiana* leaves. Total ZmSIP3-4myc protein lacking protease inhibitor were mixed
960 in different proportions with mCherry-6HA or UmSee1ΔSP-mCherry-6HA protein
961 extracts either in the presence of 100 μM MG132 or DMSO (control) and incubated at
962 28°C for 45 min before the reactions were stopped by boiling samples at 95°C in 2xSDS
963 loading buffer for 10 min. Samples were analyzed by western blot using anti-myc and
964 anti-HA as indicated. Coomassie brilliant blue (CBB) staining served as loading control.
965 (**E**) Hypothetical model for the function of UmSee1. *U. maydis* secretes UmSee1
966 protein which binds to ZmSGT1 and ZmSIPs (ZmSIP1, ZmSIP2, ZmSIP3) to modify
967 the SCF complex and enhance proteasome activity, affecting the degradation of cell
968 cycle-related proteins, including ZmSIP3.
969

970 **Supporting Information**

971 **Fig S1: UmSee1 interacting proteins enrichment by TurboID-based biotin**
972 **labelling.**

973 **Fig S2: Protein-protein interaction (PPIs) analysis of proteins that were**
974 **specifically identified in UmSee1 samples.**

975 **Fig S3: Gene Ontology (GO) analysis of proteins that were specifically identified**
976 **in UmSee1 samples.**

977 **Fig S4: Identified ZmSIPs (ZmSIP1, ZmSIP2, ZmSIP3).**

978 **Fig S5: Subcellular localization of ZmSIPs and UmSee1 upon expression in**
979 ***Nicotiana benthamiana*.**

980 **Fig S6: Y2H assays involving SrSee1 and UhSee1 and the ZmSIPs.**

981

982 **Table S1: Primers used in this study.**

983 **Table S2: Fungal strains used in this study.**

984 **Table S3: Quantification of infection symptoms on maize seedlings at 12 dpi.**

985 **Table S4: Mass spectrometry data of UmSee1.**

986 **Table S5: List of identified UmSee1-interacting proteins.**

987

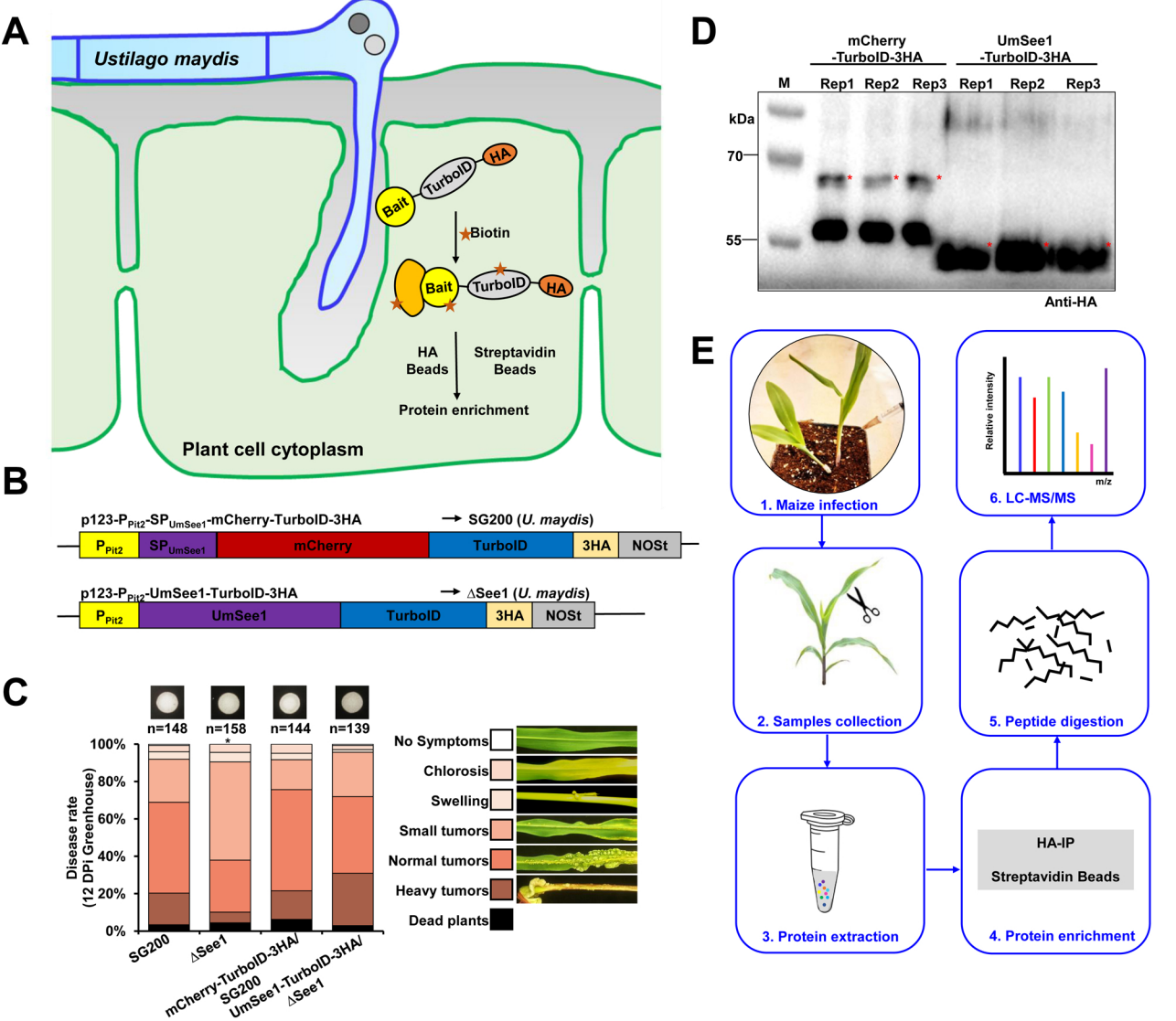
A
Ustilago maydis
Bait
TurboID
HA
Biotin
Bait
TurboID
HA
HA Beads
Streptavidin Beads
Protein enrichment
Plant cell cytoplasm
B
p123-P$_{Pit2}$-SP$_{UmSee1}$-mCherry-TurboID-3HA
→ SG200 (U. maydis)
P$_{Pit2}$
SP$_{UmSee1}$
mCherry
TurboID
3HA
NOSt
p123-P$_{Pit2}$-UmSee1-TurboID-3HA
→ ΔSee1 (U. maydis)
P$_{Pit2}$
UmSee1
TurboID
3HA
NOSt
C
n=148
n=158
n=144
n=139
100%
80%
60%
40%
20%
0%
Disease rate
(12 DPi Greenhouse)
SG200
ΔSee1
mCherry-TurboID-3HA/ SG200
UmSee1-TurboID-3HA/ ΔSee1
No Symptoms
Chlorosis
Swelling
Small tumors
Normal tumors
Heavy tumors
Dead plants
D
mCherry -TurboID-3HA
UmSee1 -TurboID-3HA
M
Rep1
Rep2
Rep3
Rep1
Rep2
Rep3
kDa
70
55
Anti-HA
E
1. Maize infection
2. Samples collection
3. Protein extraction
HA-IP
Streptavidin Beads
4. Protein enrichment
5. Peptide digestion
Relative intensity
m/z
6. LC-MS/MS

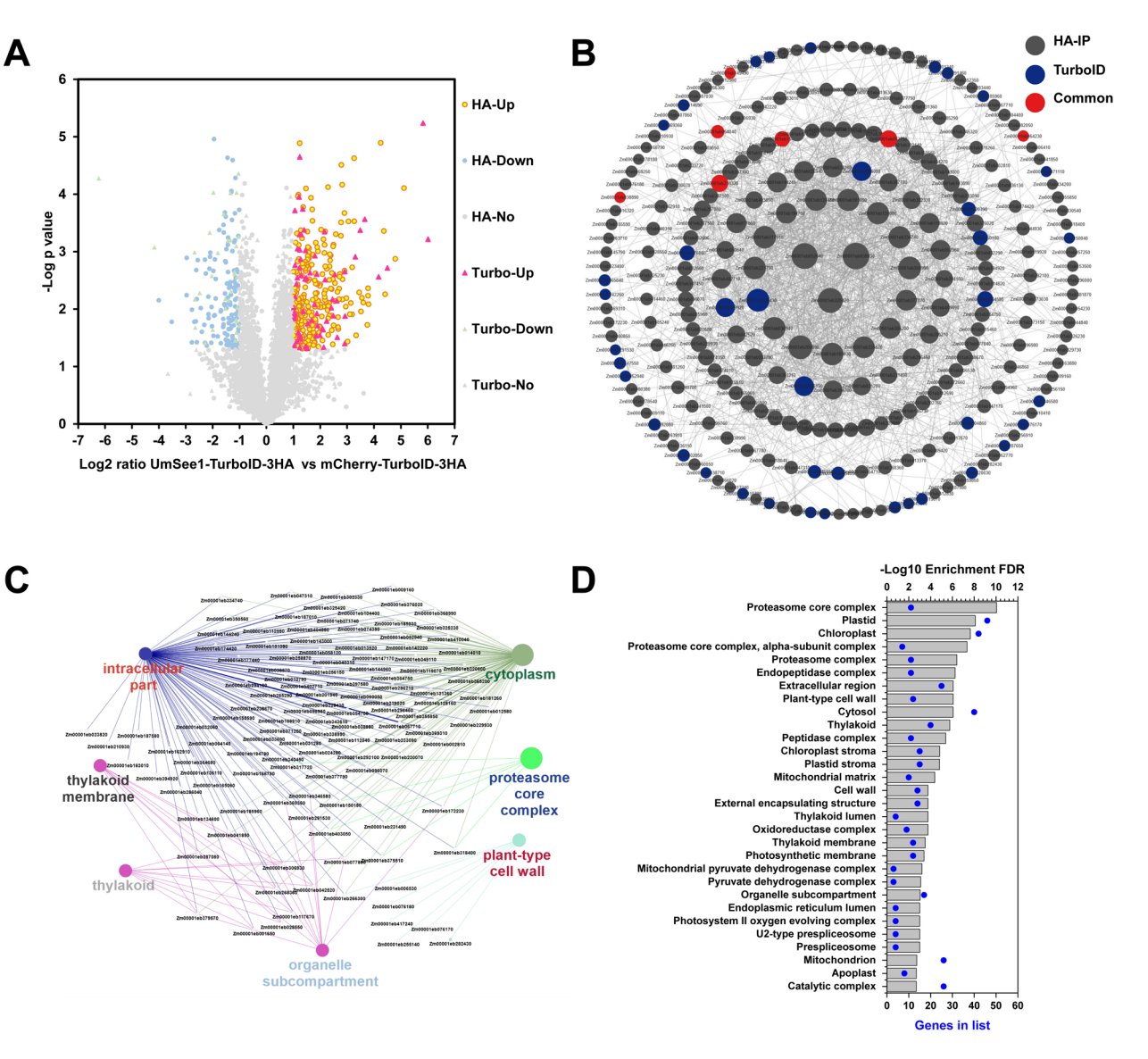
A
-Log p value
Log2 ratio UmSee1-TurboID-3HA vs mCherry-TurboID-3HA
HA-Up
HA-Down
HA-No
Turbo-Up
Turbo-Down
Turbo-No
B
HA-IP
TurboID
Common
C
intracellular part
cytoplasm
thylakoid membrane
proteasome core complex
plant-type cell wall
thylakoid
organelle subcompartment
D
-Log10 Enrichment FDR
Proteasome core complex
Plastid
Chloroplast
Proteasome core complex, alpha-subunit complex
Proteasome complex
Endopeptidase complex
Extracellular region
Plant-type cell wall
Cytosol
Thylakoid
Peptidase complex
Chloroplast stroma
Plastid stroma
Mitochondrial matrix
Cell wall
External encapsulating structure
Thylakoid lumen
Oxidoreductase complex
Thylakoid membrane
Photosynthetic membrane
Mitochondrial pyruvate dehydrogenase complex
Pyruvate dehydrogenase complex
Organelle subcompartment
Endoplasmic reticulum lumen
Photosystem II oxygen evolving complex
U2-type prespliceosome
Prespliceosome
Mitochondrion
Apoplast
Catalytic complex
Genes in list

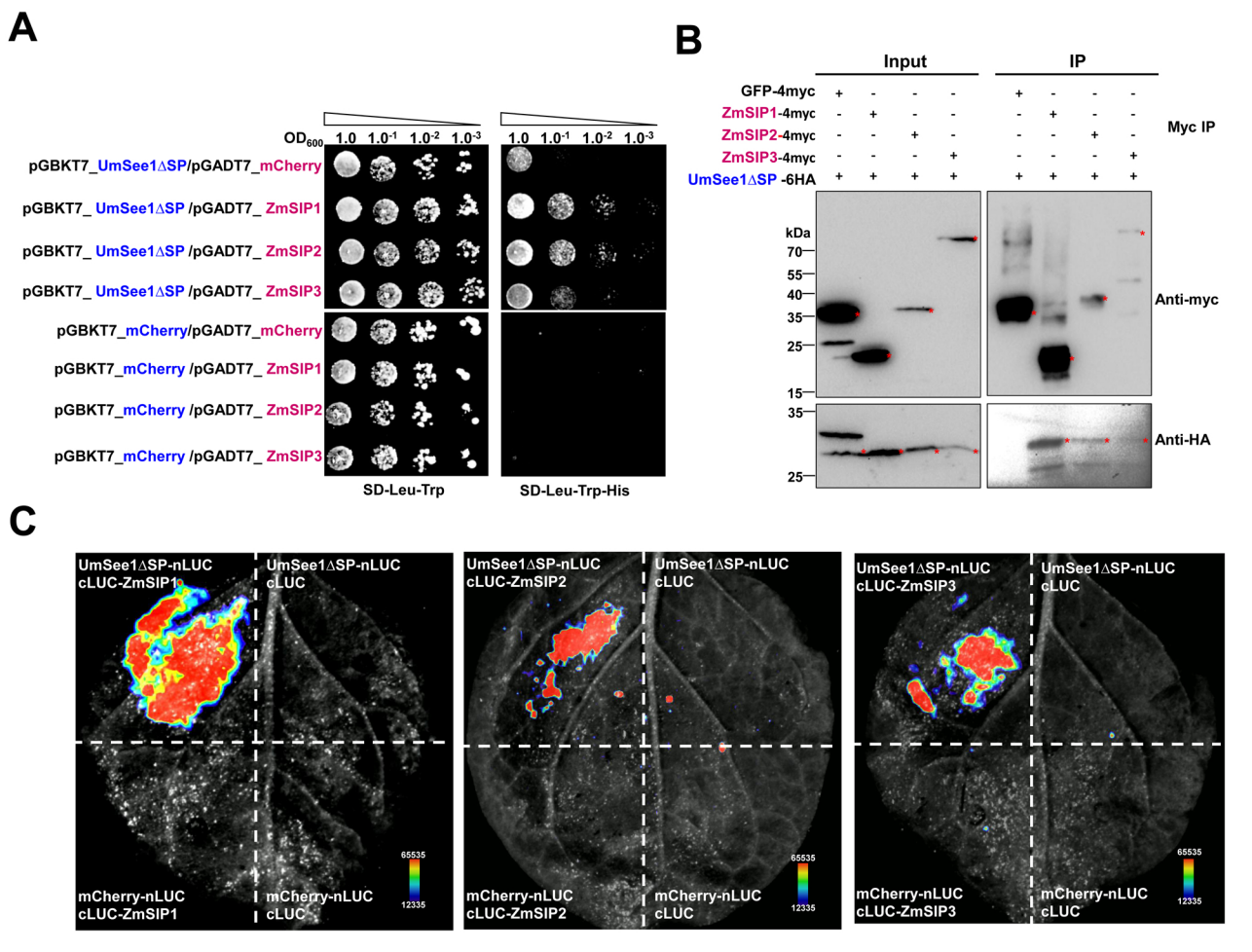
A
OD600
1.0 1.0-1 1.0-2 1.0-3
pGBKT7_UmSee1ΔSP/pGADT7_mCherry
pGBKT7_ UmSee1ΔSP /pGADT7_ ZmSIP1
pGBKT7_ UmSee1ΔSP /pGADT7_ ZmSIP2
pGBKT7_ UmSee1ΔSP /pGADT7_ ZmSIP3
pGBKT7_mCherry/pGADT7_mCherry
pGBKT7_mCherry /pGADT7_ ZmSIP1
pGBKT7_mCherry /pGADT7_ ZmSIP2
pGBKT7_mCherry /pGADT7_ ZmSIP3
SD-Leu-Trp
SD-Leu-Trp-His
B
Input
IP
GFP-4myc
ZmSIP1-4myc
ZmSIP2-4myc
ZmSIP3-4myc
UmSee1ΔSP -6HA
Myc IP
kDa
70
55
40
35
25
15
Anti-myc
Anti-HA
C
UmSee1ΔSP-nLUC
cLUC-ZmSIP1
UmSee1ΔSP-nLUC
cLUC
mCherry-nLUC
cLUC-ZmSIP1
mCherry-nLUC
cLUC
UmSee1ΔSP-nLUC
cLUC-ZmSIP2
UmSee1ΔSP-nLUC
cLUC
mCherry-nLUC
cLUC-ZmSIP2
mCherry-nLUC
cLUC
UmSee1ΔSP-nLUC
cLUC-ZmSIP3
UmSee1ΔSP-nLUC
cLUC
mCherry-nLUC
cLUC-ZmSIP3
mCherry-nLUC
cLUC
65535
12335

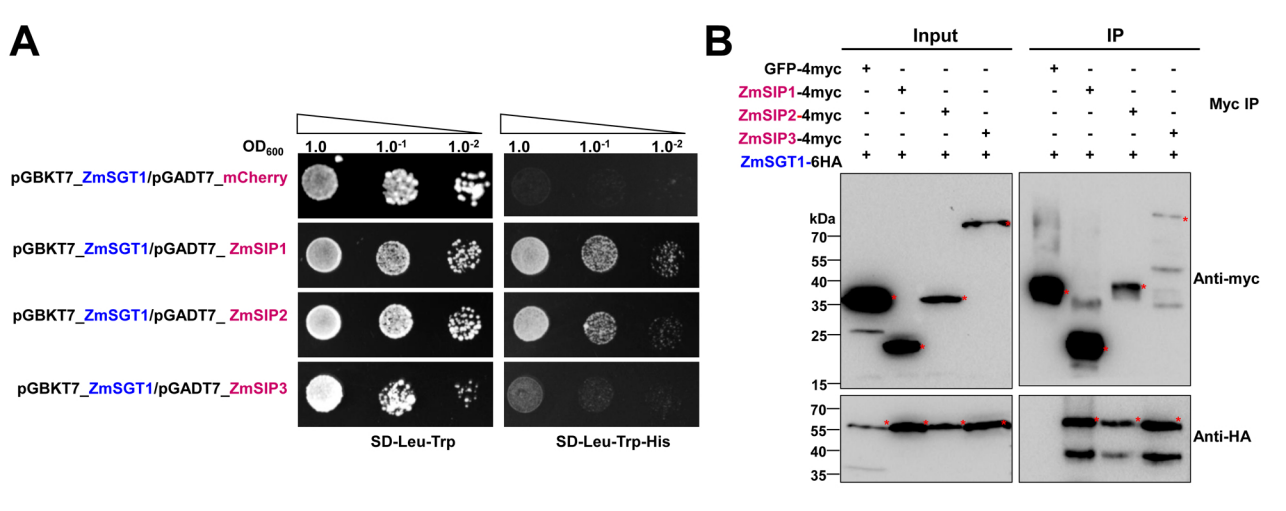
A
OD600
1.0
1.0-1
1.0-2
1.0
1.0-1
1.0-2
pGBKT7_ZmSGT1/pGADT7_mCherry
pGBKT7_ZmSGT1/pGADT7_ ZmSIP1
pGBKT7_ZmSGT1/pGADT7_ ZmSIP2
pGBKT7_ZmSGT1/pGADT7_ZmSIP3
SD-Leu-Trp
SD-Leu-Trp-His
B
Input
IP
GFP-4myc
ZmSIP1-4myc
ZmSIP2-4myc
ZmSIP3-4myc
ZmSGT1-6HA
Myc IP
kDa
70
55
40
35
25
15
Anti-myc
70
55
40
35
Anti-HA

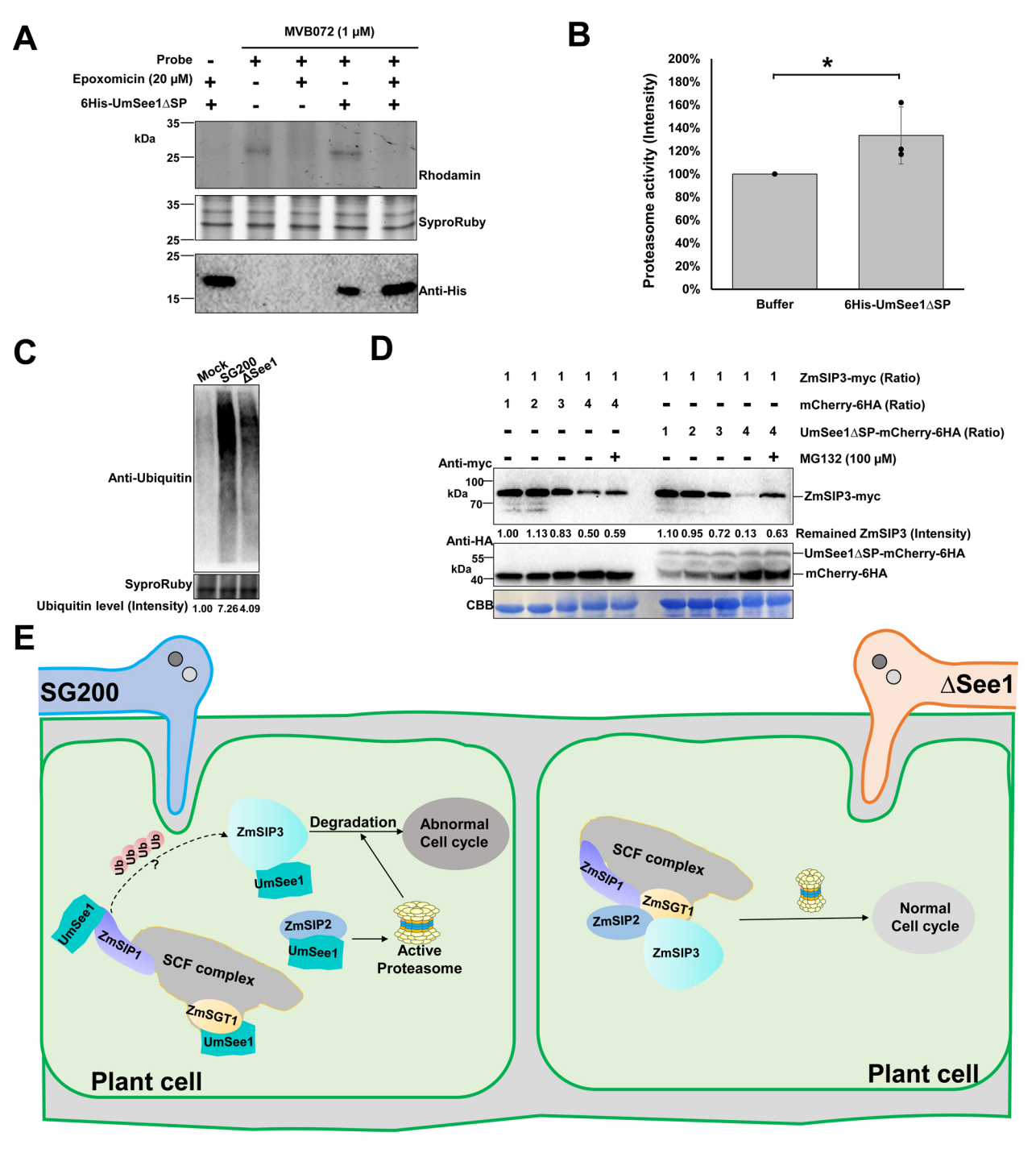
A
MVB072 (1 μM)
Probe - + + + +
Epoxomicin (20 μM) + - + - +
6His-UmSee1ΔSP + - - + +
kDa
35
25
Rhodamin
35
25
SyproRuby
25
15
Anti-His
B
Proteasome activity (Intensity)
200%
180%
160%
140%
120%
100%
80%
60%
40%
20%
0%
*
Buffer
6His-UmSee1ΔSP
C
Mock
SG200
ΔSee1
Anti-Ubiquitin
SyproRuby
Ubiquitin level (Intensity) 1.00 7.26 4.09
D
ZmSIP3-myc (Ratio) 1 1 1 1 1 1 1 1 1 1
mCherry-6HA (Ratio) 1 2 3 4 4 - - - - -
UmSee1ΔSP-mCherry-6HA (Ratio) - - - - - 1 2 3 4 4
MG132 (100 μM) - - - - + - - - - +
Anti-myc
100
kDa
70
ZmSIP3-myc
1.00 1.13 0.83 0.50 0.59 1.10 0.95 0.72 0.13 0.63 Remained ZmSIP3 (Intensity)
Anti-HA
55
kDa
40
UmSee1ΔSP-mCherry-6HA
mCherry-6HA
CBB
E
SG200
ΔSee1
Ub Ub Ub Ub
?
ZmSIP3
Degradation
Abnormal Cell cycle
UmSee1
UmSee1
ZmSIP1
SCF complex
ZmSIP2
UmSee1
Active Proteasome
ZmSGT1
UmSee1
Plant cell
SCF complex
ZmSIP1
ZmSGT1
ZmSIP2
ZmSIP3
Normal Cell cycle
Plant cell